Uplifting of carbon monoxide from biomass burning and anthropogenic sources to the free troposphere in East Asia

K. Ding[1,6], J. Liu[1,2,6,*], A. Ding[1,6], Q. Liu[1,6], T. L. Zhao[3], J. Shi[4], Y. Han[1], H. Wang[5], F. Jiang[5]

[1]School of Atmospheric Sciences, Nanjing University, Nanjing, Jiangsu, 210093, China

[2]University of Toronto, Toronto, Ontario, M5S 3G3, Canada

[3]Nanjing University of Information Science & Technology, Nanjing, Jiangsu, 210044, China

[4]Institute of Remote Sensing Applications, Chinese Academy of Sciences, Beijing, 100101, China

[5]International Institute for Earth System Sciences, Nanjing University, Nanjing, Jiangsu, 210093, China

[6]Collaborative Innovation Center of Climate Change, Jiangsu, 210093, China

To: Atmospheric Chemistry and Physics

February 2015

[*]Corresponding author

Abstract

East Asia has experienced rapid development with increasing CO emission in the past decades. Therefore, uplifting CO from the boundary layer to the free troposphere in East Asia can have great implications on regional air quality around the world. It can also influence global climate due to the longer lifetime of CO at higher altitudes. In this study, three cases of high CO episodes in the East China Sea and the Sea of Japan from 2003 to 2005 are examined with spaceborne Measurements Of Pollution In The Troposphere (MOPITT) data, in combination with aircraft measurements from the Measurement of Ozone and Water Vapor by Airbus In-Service Aircraft (MOZAIC) program. High CO abundances of 300-550 ppbv are observed in MOZAIC data in the free troposphere during these episodes. These are among the highest CO abundances documented at these altitudes. On average, such episodes with CO over 400 ppbv (in the 2003 and 2004 cases) and between 200-300 ppbv (in the 2005 case) may occur 2-5% and 10-20% in time, respectively, in the respective altitudes over the region. Correspondingly, elevated CO is shown in MOPITT daytime data in the middle to upper troposphere in the 2003 case, mostly in the lower to middle troposphere in the 2004 case, and in the upper troposphere in the 2005 case. Through analyses of the simulations from a chemical transport model GEOS-Chem and a trajectory dispersion model FLEXPART, we found different CO signatures in the elevated CO and distinct transport pathways and mechanisms for these cases. In the 2003 case, emissions from large forest fires near Lake Baikal dominated the elevated CO, which had been rapidly transported upward by a frontal system from the fire plumes. In the 2004 case, anthropogenic CO from the North China Plain experienced

frontal lifting and mostly reached ~700 hPa near the East China Sea, while CO from biomass burning over Indochina experienced orographic lifting, leeside-trough induced convection, and frontal lifting through two separate transport pathways, leading to two distinct CO enhancements around 700 hPa and 300 hPa. In the 2005 case, the observed CO of ~300 ppbv around 300 hPa originated from anthropogenic sources over the Sichuan basin and the North China Plain and from forest fires over Indochina. The high CO was transported to such altitudes through strong frontal lifting, interacting with convection and orographic lifting. These cases show that topography affects vertical transport of CO in East Asia via different ways, including orographic uplifting over the Hengduan Mountains, assisting frontal lifting in the North China Plain, and facilitating convection in the Sichuan basin. In particular, topography-induced leeside troughs over Indochina led to strong convection that assisted CO uplifting to the upper troposphere. This study shows that the new daytime MOPITT near-infrared (NIR) and thermal-infrared (TIR) data (version 5 or above) have enhanced vertical sensitivity in the free troposphere and may help qualitative diagnosis of vertical transport processes in East Asia.

1 Introduction

Carbon monoxide (CO) plays several important roles in the atmosphere. The oxidizing capability, an ability of the atmosphere to cleanse itself, is strongly influenced by the CO level in the troposphere. CO near the surface is a major pollutant. Under high NO_x conditions, CO is a precursor of ozone, while in low NO_x airmasses, CO helps ozone destruction (Jacob, 1999; Holloway et al., 2000). As carbon dioxide (CO_2) is produced in

47 both ozone production and destruction processes (Holloway et al., 2000), CO is linked to
48 the global carbon cycle (Suntharalingam et al., 2004; Yurganov et al., 2008; Nassar et al.,
49 2010) affecting climate change. With a lifetime of weeks to months, CO is a good tracer
50 tracking transport of pollution. In the purview of these roles, it is important to understand
51 processes influencing the CO distribution and variability in the atmosphere.

52 Although the main sources of atmospheric CO and its mean status are generally
53 understood (Novelli et al., 1998; Jacob, 1999; Holloway et al., 2000), many processes
54 influencing CO variations at different time scales are not well known. Uplifting CO from
55 the boundary layer to the free troposphere (FT) is such a process, which usually occurs on
56 the synoptic scale that spans hundreds to thousands of kilometers in space and lasts hours
57 to days in time (Daley, 1991). Uplifted CO usually has a longer lifetime and can be
58 transported fast by the upper layer winds over long distances through continents and
59 between hemispheres in the troposphere (Stohl, 2001; Stohl et al., 2002; Damoah et al.,
60 2004). Uplifting airmass from the surface to FT generally takes place by three processes
61 (1) frontal lifting, (2) orographic lifting, and (3) deep convection (Brown et al., 1984;
62 Banic et al., 1986; Dickerson et al., 1987; Bethan et al., 1998; Pickering et al., 1998;
63 Chung et al., 1999; Donnell et al., 2001; Kowol-Santen et al., 2001;Cooper et al., 2002;
64 Liu et al., 2003; Miyazaki et al., 2003; Chan et al.; 2004; Mari et al., 2004; Li et al., 2005;
65 Liu et al., 2006; Kar et al., 2008; Zhao et al., 2008; Ding et al., 2009; Randel et al., 2010;
66 Chen et al., 2012).

67 East Asia has experienced rapid development with increasing CO emission in the
68 past decades (Duncan et al., 2007). In addition to impacts on local air quality (Wang et al.,
69 2010), continuing increase in CO emissions will lead to great impacts on regional air

quality and climate of the world (Jaffe et al., 1999; Berntsen et al., 1999; Bertschi et al., 2004) because of an expected upward trend in pollution outflow from the region. East Asia is characterized by its unique and complex meteorology, topography, and land covers. Vertical transport of CO can be modulated by one or more of these conditions or by their interactions. For example, the likelihood of when and where extratropical cyclones are active is closely linked to the locations and frequency of frontal uplifting. Wet and dry convections prevail in different seasons in northern China because of the distinct climatological pattern in precipitation there (Dickerson et al., 2007). The topography there also plays an important role in uplifting of CO alone and/or interplaying with frontal systems, aiding convection in mountainous regions (Liu et al., 2003; Ding et al. 2009). Recently, Lin et al. (2009) proposed a new mechanism that emphasizes the role of topography-induced leeside troughs over Indochina in promoting strong convection. A variety of land cover types in East Asia diversifies CO sources there. In highly populated urban areas, such as those in the North China Plain, anthropogenic emissions are high. Large biomass burning, occurring in areas with abundant vegetation, can generate great amounts of CO for vertical transport when meteorological conditions become favorable. Two such areas are Southeast Asia and the boreal forested area in Russia (Wotawa et al., 2001; Schultz, 2002; Duncan et al., 2003). So far, our understanding of the impacts of these processes and their interactions on CO uplifting is still rather limited (Dickerson et al., 2007). The objectives of studying vertical transport of CO in East Asia are to better understand the vertical distribution of CO in the region, to advance the assessment of impacts of long-range transport of Asian CO on regions downwind, and to help improve simulating this process in atmospheric models on the synoptic scale, eventually leading to

more realistic chemical weather forecast in the future (Lawrence et al., 2003).

Due to lack of continuous measurements, most studies on CO in East Asia are based on observations from periodic field campaigns (Jacob et al., 2003; Tsutsumi et al., 2003; Li et al., 2007; Ding et al., 2009) or simulations by chemical transport models (Berntsen et al., 1999; Bey et al., 2001) or both (Liu et al., 2003). CO measurements from satellites provide unprecedented data revealing CO variations over East Asia. One of the instruments is the Measurements Of Pollution In The Troposphere (MOPITT) (Drummond, 1992; Drummond and Mond, 1996). MOPITT provides data of CO total column and CO vertical profiles at several altitude levels, which are retrieved using a nonlinear optimal estimation method theoretically based on the observed radiances and their weighting functions, the a priori information, and the retrieval averaging kernels (Rogers, 2000; Deeter et al., 2003). As a result, the MOPITT retrieval at one level can be influenced by CO at other levels and thus MOPITT vertical resolution is coarse, generally having only 2-3 pieces of independent information vertically in the troposphere. Therefore, MOPITT's vertical sensitivity was an issue with earlier versions of MOPITT data (Jacob et al., 2003). Nevertheless, a few studies (Deeter et al., 2004; Kar et al., 2004, 2006, 2008; Liu et al., 2006) demonstrated MOPITT's vertical sensitivity to some extent. Kar et al. (2004) found Asian summer monsoon plumes in MOPITT CO data as a strong enhancement of CO in the upper troposphere over India and southern China. Deeter et al. (2004) illustrated similar distributions of the rain rate and the ratio of MOPITT CO at 350 hPa to at 850 hPa in the Tropical Eastern Pacific Ocean. Liu et al. (2006) observed large differences (20-40 ppbv) in MOPITT CO at 250 hPa between two cases of vertical transport of CO and attributed the differences to the respective weather systems.

Furthermore, the MOPITT data in new versions that use both thermal infrared and near infrared radiances have offered enhanced vertical sensitivity (Worden et al., 2010; Deeter et al., 2012; 2013). Therefore, a detailed examination of MOPITT's vertical sensitivity in East Asia, especially for its ability in detecting vertical transport of high CO episodes, is desirable.

In this study, three cases of high CO episodes in East Asia from 2003 to 2005 are examined with MOPITT satellite data, in combination with aircraft measurements from the Measurement of Ozone and Water Vapor by Airbus In-Service Aircraft (MOZAIC) program (Marenco et al.,1998) (see Sects.2 and 4). The vertical transport mechanisms are analyzed with simulations from a trajectory dispersion model FLEXPART (Stohl et al., 2005) and a chemical transport model GEOS-Chem (Bey et al.,2001), along with other meteorology data and satellite fire data (see Sects.2 and 4). MOPITT data are analyzed in two ways. First, the vertical sensitivity of MOPITT is evaluated with the coincident MOZAIC data (see Sect.3) and further illustrated with the three high CO episodes in comparison with the MOZAIC data (see Sect.4). Second, the vertical variation in CO captured by MOPITT is used to diagnose vertical transport of CO (see Sect. 4). Discussion on the three cases is synthesized in Sect.5 and the major conclusions are provided in Sect.6.

2 Model and data

2.1 Satellite MOPITT CO data

MOPITT is the first space instrument that targets continuous measurements of tropospheric CO. MOPITT has been onboard of the Terra satellite since 1999, making

scientific measurements since March 2000.Terra is flying in a sun synchronous polar orbit with an altitude of 705 km, crossing the equator at ~10:45 and 22:45 local time and making 14-15 daytime and nighttime overpasses each day. MOPITT uses a cross-track scanning method with a swath of 29 pixels (4 pixels in a row), each pixel being 22 km × 22 km. Therefore, with a swath of ~600 km, about one third of the global area is covered in a day. Additionally, clouds can cause even more gaps in MOPITT daily data. This makes it challenging to use MOPITT data for synoptic studies. It takes 3 days to achieve a near-complete global coverage (Edwards et al., 1999) assuming no blockage from clouds.

MOPITT measures upwelling radiation in two narrow infrared spectral regions for CO retrieval: (1) a thermal-infrared (TIR) band near 4.7 μm that has strong carbon monoxide absorption and (2) a near-infrared (NIR) band near 2.3 μm that has weak CO absorption. MOPITT Version 5 retrieval products are significantly different from earlier products and offer three distinct products depending on application requirements. One of them is a TIR/NIR "multispectral" product, which has enhanced sensitivity to CO in the lower-most troposphere (Worden et al., 2010; Deeter et al., 2012; 2013). Validations and evaluations of MOPITT data in various versions are documented in Emmons et al. (2004), Worden et al. (2010), and Deeter et al. (2012, 2013).

In this study, the MOPITT CO profiles (Level 2 data) were first compared with the coincident MOZAIC profiles. Advances of Version 5 (V5, a TIR/NIR "multispectral" product) from Version 4 (V4, a TIR-only product) data were assessed. Then, the V5 data were used in the case studies, in which MOPITT Level 2 data were gridded horizontally into 0.25 °latitude × 0.25 °longitude bins and vertically at the MOPITT resolution of 100

hPa from the surface to 100 hPa.

2.2 Aircraft MOZAIC CO data

The MOZAIC program was initiated in 1993 by European scientists, aircraft manufacturers, and airlines to collect experimental data (Marenco et al., 1998). MOZAIC consists of automatic and regular measurements of ozone, CO, and water vapor by several long range passenger airliners flying all over the world. The aim is to build a large database of measurements to allow studies of chemical and physical processes in the atmosphere.

In comparing MOPITT with MOZAIC CO data, coincident MOPITT and MOZAIC data from 2003 to 2005 were screened within a radius of 1.5 °and within a 4 h period. The radius of 1.5 °was applied to selected MOZAIC profiles at 500 hPa and the MOZAIC slant path was included in the radius. MOZAIC profile was smoothed by applying the MOPITT averaging kernels and the a priori profile for the co-located retrieved MOPITT profile to account for the bias introduced by the averaging kernels and the a priori. Therefore, the smoothed MOZAIC CO profile $\hat{\mathbf{x}}^{MOZAIC}$ is derived by (Rogers, 2000)

$$\hat{\mathbf{x}}^{MOZAIC\_MOPITT} = \mathbf{x}_{\mathbf{a}}^{MOPITT} + \mathbf{A}\left(\mathbf{x}^{MOZAIC\_MOPITT} - \mathbf{x}_{\mathbf{a}}^{MOPITT}\right) \quad (1)$$

where $\mathbf{A} = \partial\hat{\mathbf{x}}/\partial\mathbf{x}$ is the MOPITT averaging kernel matrix which describes the sensitivity of the MOPITT CO estimate to the true profile of CO, $\mathbf{x}^{MOZAIC}$ is the MOZAIC CO profile, which has been mapped to the MOPITT pressure grid. The quantity $\mathbf{x}_{\mathbf{a}}^{MOPITT}$ is the MOPITT a priori, which is based on CO simulations from the MOZART model (Emmons et al., 2004).

The MOZAIC measurements usually extend from the surface to ~ 250 hPa. When validating MOPITT data using Eq.(1), CO mixing ratios above 300 hPa was supplemented with CO from the GEOS-Chem chemical transport model (see Sect.2.6) on the same location and day, similar to the treatments by Worden et al.(2010), who used the MOZART climatology simulations. Because CO above 250 hPa is lower than that in the middle and lower troposphere, the bias due to this treatment is expected to be low.

2.3 MODIS fire count data

The Moderate-resolution Imaging Spectroradiometer (MODIS) is a type of instruments which have been onboard of the Terra (EOS AM) satellite since 1999 and on the Aqua (EOS PM) satellite since 2002. The MODIS fire products include a validated daily global active fire product (MOD14 Terra and MYD14 Aqua) (Justice et al., 2002), generated using a global active fire detection algorithm that uses a multispectral contextual approach to exploit the strong emission of midinfrared radiation from fires allowing subpixel fire detection (Giglio et al., 2003). The horizontal resolution is 1 km. The fire data are acquired from the Fire Information for Resource Management System (FIRMS) (Davies et al., 2009).

2.4 NCEP FNL meteorological data

The NCEP Final (FNL) global tropospheric analyses are on 1 °by 1 °grids every 6h (http://rda.ucar.edu/datasets/ds083.2/). Parameters in FNL include surface pressure, sea level pressure, geopotential height, temperature, sea surface temperature, potential temperature, relative humidity, precipitable water, u and v winds, and vertical motion,

209 available on the surface, at 26 levels from 1000 to 10 hPa, the tropopause, the boundary
210 layer, and a few others. In addition to driving FLEXPART (see Sect. 2.5), the FNL data
211 are used to analyze the meteorological conditions including the surface pressure, wind
212 fields, and development of a cyclone. The data are generated from the Global Data
213 Assimilation System (GDAS).
214

215 ## 2.5 The FLEXPART trajectory model

216 To diagnose the transport processes and trace CO sources, we used the FLEXPART
217 model (Stohl et al., 2005), which is a Lagrangian Particle Dispersion Model developed at
218 the Norwegian Institute for Air Research in the Department of Atmospheric and Climate
219 Research. FLEXPART can be driven by meteorological input data generated from a
220 variety of global and regional models. In this study, the simulations were driven by the
221 NCEP FNL data. This model has been extensively validated (Stohl et al., 1998;
222 Cristofanelli et al., 2003) and widely used in studies of the influence of various
223 meteorological processes on pollution transport (Cooper et al., 2004, 2005, 2006;
224 Hocking et al., 2007; Ding et al., 2009; Barret et al., 2011; He et al., 2011; Chen et al.,
225 2012). In running FLEXPART, a large number of particles are released from defined
226 locations (latitude, longitude, and altitude) at a time. Backward or forward trajectories of
227 the particles are recorded in latitude (°), longitude (°), and altitude (km) every hour.
228

229 ## 2.6 The GEOS-Chem chemical transport model

230 GEOS-Chem is a global three dimensional chemical transport model
231 (http://geos-chem.org). The model contains detailed description of tropospheric

O3-NOx-hydrocarbon chemistry, including the radiative and heterogeneous effects of aerosols. It is driven by assimilated meteorological observations from the National Aeronautics and Space Administration (NASA) Goddard Earth Observing System (GEOS) from the Global Modeling and Assimilation Office (GMAO). In this study, GEOS-Chem version v9-1-3 was employed and executed in the full chemistry mode, which is driven by GEOS meteorology with temporal resolution of 6h (3h for surface meteorological variables), with a horizontal resolution of 2 °latitude by 2.5 °longitude and 47 vertical levels, including ~35 levels in the troposphere from 1000 to 100 hPa.

GEOS-Chem uses anthropogenic emissions from the Emissions Database for Global Atmospheric Research (EDGAR) global inventory (Olivier and Berdowski, 2001), which are updated with regional inventories, including the emission inventory in Asia (Streets et al., 2006; Zhang et al., 2009). The biomass burning emissions are from the Global Fire Emissions Data (GFEDv3) monthly inventories (van der Werf et al., 2010) and biogenic VOC emissions are taken from the Model of Emissions of Gases and Aerosols from Nature (MEGAN) global inventory. Emissions from other natural sources (e.g., lightning, volcanoes) are also included.

The model has been extensively evaluated and used in studies of atmospheric chemistry and pollution transport (Bey et al., 2001; Heald et al., 2003; Liu et al., 2003; Liu et al., 2006; Zhang et al., 2006; Jones et al., 2009; Nassar et al., 2009; Kopacz et al., 2010; Jiang et al., 2011). GEOS-Chem can generally describe CO variability in the troposphere but somewhat underestimate the observations in the northern mid-latitudes possibly due to biases in the CO inventory or numerical diffusion in the model or both (Heald et al., 2003; Duncan et al., 2007; Nassar et al., 2009; Kopacz et al., 2010).

255

256 3 Comparison between MOPITT and MOZAIC CO profiles

257 MOPITT's vertical sensitivity can be described in terms of the averaging kernels
258 (see Eq.1) and the Degree of Freedom for Signal (DFS). The averaging kernel matrix
259 indicates the sensitivity of the MOPITT CO estimate to the true CO profile, with I
260 (identity matrix) being the best, when true CO profiles are retrieved, and 0 being the
261 worst, when MOPITT retrievals just take the a priori. In reality, the average kernel matrix
262 is less than I, implying some contribution of CO from other levels to the retrieved level so
263 that the CO vertical structure cannot be fully resolved. DFS gives the number of
264 independent pieces of information available vertically in the measurements and it is the
265 sum of the diagonal elements of the averaging kernel matrix (Rogers, 2000). Figure 1
266 shows a yearly mean of DFS for daytime and nighttime, respectively, in East Asia for the
267 V5 TIR/NIR data, indicating substantial increases in DFS compared to earlier MOPITT
268 versions (Worden et al., 2010; Deeter et al., 2012). The daytime DFS in East Asia (Fig.1a)
269 ranges from 0.5 to 2.7, usually decreasing with latitude, similar to its distribution in other
270 regions and on the global scale (Deeter et al., 2004; Worden et al., 2010). In the same
271 latitudinal zones, the DFS is higher over land than over ocean. The daytime annual DFS
272 is high in the Sichuan basin, the eastern part of mainland China, the Indochina peninsula,
273 and the Indian subcontinent. Over the mountain or valley regions, DFS is low, such as
274 above the Tibetan Plateau. The stars indicate the cities where MOZAIC vertical
275 measurements are available for validation of MOPITT data. The annual mean DFS is
276 1.65, 1.51, 1.60, and 1.64, respectively, in an area of 1 °x1 °around Beijing, Narita,
277 Shanghai, and Hong Kong, with a maximum of 1.98, 1.64, 1.81, and 1.74 for the cities,

278 respectively. The nighttime DFS values (Fig. 1b) are lower (from 0.5 to 1.5) than the
279 daytime values, similar to that in Deeter et al. (2004) for an earlier MOPITT version.
280 Spatially, nighttime DFS is high over regions where the daytime DFS is also high.

281 The general patterns of MOPITT averaging kernels have been documented (Pan et
282 al., 1998; Emmons et al., 2004; Deeter et al., 2003, 2004, 2012; Kar et al., 2008; Worden
283 et al., 2010). For V5 MOPITT data, the averaging kernels at the four cities are similar to
284 these in Worden et al. (2010, in their Fig. 7). The difference in the averaging kernels
285 between V4 and V5 can be as large as 0.14 in the surface and lower troposphere and as
286 0.10 in the upper troposphere (not shown).

287 Figure 2 shows the relative bias between MOPITT and the smoothed MOZAIC
288 $(\hat{\mathbf{x}}^{MOZAIC})$ profiles (see Eq. 1), which is also referred as "MOPITT estimate of in situ" in
289 Worden et al. (2010) and "transferred profile" in Emmons et al. (2004). For V5 data (in
290 red), the mean bias is within ±20% for all the cities. In all the altitude levels, the bias is
291 smallest (close to zero) around 500-400 hPa and increases upward and downward. The
292 bias is mostly positive above 500-400 hPa, while below 500-400 hPa, it is positive at
293 Beijing, Narita but negative at Shanghai and Hong Kong. Whether the sign change is
294 related to the change in the geographic location (Shanghai and Hong Kong are both
295 coastal cities) can be a subject for further study. The V4 data (in green) also show the
296 smallest bias in the middle troposphere. In the lower troposphere, the bias in V5 is
297 reduced by 5-10% at Beijing and Narita. At Shanghai and Hong Kong, the bias changes
298 from positive in V4 to negative in V5, with a smaller (at Shanghai) or larger (at Hong
299 Kong) magnitude. In the upper troposphere above 500-400 hPa, the bias in V5 at Beijing,
300 Narita, and Shanghai changes to positive, with a magnitude similar to or larger than that

in V4. At Hong Kong, the bias in V5 remains positive but the magnitude is enlarged. Deeter et al. (2013) compared MOPITT data with the NOAA aircraft measurements over North America and data from the HIAPER Pole to Pole Observations (HIPPO) field campaign data (Wofsy et al., 2011). They found a positive bias in MOPITT V5 TIR/NIR data at 400 hPa (4%) and 200 hPa (14%). They also showed a latitude-dependent positive bias in the northern hemispherical upper troposphere in MOPITT V3 and V4 data. This study suggests an overall positive bias, agreeing with Deeter et al. (2013) in magnitude and sign, in MOPITT V5 data for the upper troposphere. As a comparison, we also validated MOPITT data in other cities in the globe and found that the mean bias in Europe or the United States is lower than that in East Asia, especially in the surface layer (not shown).

The correlation between MOPITT and smoothed MOZAIC data is shown in Fig. 3. From 500 to 100 hPa, the correlation coefficient between the two data sets is 0.92, 0.86, 0.83, 0.68 at Beijing, Narita, Shanghai, and Hong Kong, respectively (Fig.3a), while from the surface to 600 hPa, the correlation becomes stronger, being 0.90,0.92, 0.92, 0.94 at Beijing, Narita, Shanghai, and Hong Kong, respectively (Fig. 3b). The correlation coefficient between the two data is the best in the middle troposphere (500-400 hPa, not shown).

4 Uplifting of CO to the free troposphere

Daily MOPITT and MOZAIC data from 2003-2005 were screened to find cases of high CO episodes observed by both MOPITT and MOZAIC at the same location and time. We found three cases of high CO in MOPITT data with close-by MOZAIC

measurements, while it was hard to find such high CO episodes with exact coincident MOPITT and MOZAIC observations because of large gaps in MOPITT data and limited aircraft sampling coverages. In the three cases, high CO concentrations up to 300-500 ppbv were observed by MOZAIC in the free troposphere from 750 to 350 hPa.

In the following, we provide detailed analyses of each case, ordered by year of occurrence (Table 1). The cases occurred over the East China Sea or the Sea of Japan or both. High CO was shown in MOPITT daytime data in the middle to upper troposphere in case 2003, mostly in the lower to middle troposphere in case 2004, and in the upper troposphere in case 2005. The MOPITT and MOZAIC observations for the three cases are shown in Figs. 4-6, followed by analyses for each case with FLEXPART and GEOS-Chem simulations, in combination with MODIS fire data and NCEP FNL meteorological data. The cases occurred in spring and summer when cyclone activities are strong in East Asia (Chen et al., 1991; Yue and Wang, 2008). The main CO sources are identified as biomass burning or a combination of biomass burning and anthropogenic origins. The outflow of the high CO episodes finally reached the boundary layer at the west coast of the United States and Canada.

4.1 Case study I: 6 June 2003

On 6 June 2003, a large area (~ 400 km × 1500 km) of high CO up to 350 ppbv appeared in the MOPITT image over the Sea of Japan and the nearby continent in the middle to high troposphere (Fig. 4a). In Fig. 5a, the MOPITT CO profile averaged over the boxed area in Fig. 4a shows a broad enhancement from the monthly profile between 650-300 hPa, with peak CO abundances of ~300 ppbv around 550 hPa. The location and

shape of the box was selected to ensure enough MOPITT samplings (>30) at the closest upwind direction of MOZAIC measurements (the same for Figs. 4b and 4c). The large difference between the MOPITT a priori and the measurements over these altitudes indicates MOPITT's capability of detecting pollution episodes with some degree of vertical sensitivity. The vertical sensitivity is demonstrated through (1) the strongest CO source among the three cases was shown as the largest magnitude (200-250 ppbv) of elevated CO from the a priori, (2) the altitude with the maximum CO enhancement was detected around the middle troposphere, in contrast to the other two cases which show the maximum in the lower-middle and upper troposphere, respectively, and (3) the elevated CO was over a broad range of altitudes as the vertical resolution of MOPITT is rather coarse, i.e., the annual mean DFS maximizes about 2.5 (Figure 1). This CO peak was not shown in the MOPITT monthly mean profile, reflecting the episodic nature of this event. The high CO episode was also detected by a near-by MOZAIC measurement (Fig. 5b). A layer of elevated CO is apparent between 500-350 hPa, with a CO peak up to ~ 550 ppbv around 400 hPa. In addition, the MOZAIC relative humidity (RH) and ozone profiles are shown in Fig. 5b. Around the altitudes of CO buildup, elevated humidity followed the CO profile, while ozone also showed some enhancement.

A latitude-altitude cross section from MOPITT is shown in Fig. 6a. It is the average between two blue dashed lines in Fig. 4a. The arrows represent the winds in the meridional and vertical directions and the contour represents the zonal wind speed. Consistent with Fig. 4a, high CO up to 350 ppbv appeared in the middle to upper troposphere between 35-50 ºN.

To trace down the CO source, backward trajectories of the air particles were

simulated using FLEXPART after releasing 30 000 and 7000 particles, respectively, from the locations of the large and small boxed areas in Fig. 6a (the same as the blue bars in Fig. 4a) on 6 June 2003 when CO was high in the MOPITT data. Because CO has a relatively long lifetime (weeks to months), it is assumed that CO is not removed in the backward trajectories. Figure 7 shows the distribution of particle concentration between 6.25-10.25 km (~ 500-250 hPa, Fig. 7a) and between 0-3.25 km (~ 1000-650 hPa, Fig.7b). The contour lines indicate the geopotential height at 850 hPa at 12:00 UTC on 3 June 2003 (Fig. 7a) and at 0 UTC on 2 June 2003 (Fig. 7b), respectively. The locations of large forest fires near Lake Baikal from MODIS fire data are indicated in Fig. 7b by the stars, diamonds, and circles, with fire counts of 20-100, 100-300, and 300-500 per 2.5 ° × 2.5 ° grid area, respectively, averaged daily from 31 May to 6 June. The high particle counts between 0-3 km in the vicinity of Lake Baikal match well with the location of fire counts (Fig. 7b). On 3 June 2013, there was a cyclone with a cold front (Fig. 7a) that rapidly lifted the CO originated from the fires along the warm conveyer belt (WCB) to the upper level. The particle distribution in the upper troposphere shows the transport pathway of the particles to the Sea of Japan. To further illustrate this, particles were released from the fire region near Lake Baikal (93-115 °E, 50-60 °N, 0-3 km, following Lavoué et al. (2000), who found an average injection height of Siberian fires of ~ 3 km). Forward trajectories were simulated and the resultant vertical distribution of the particles, varying with time during 1-15 June 2003, is shown in Fig. 8. The released particles from the fires traveled along the isobars to northeast of Lake Baikal from 1 June to 3 June 2003 and then the particles were lifted to the upper layers (2-5 km) on 3 June at 12 a.m. (in 60-70 h) (Fig. 8). Then, the particles were transported to the east along these altitudes. On 6 June

393 (in 120-140 h), a large amount of particles appeared in a layer of 3-8 km (Figs. 8 and 4a).
394 The altitudes with high particle concentrations agree well the MOPITT data between
395 650-350 hPa (Figs. 4a and 6a).

396 It is the cyclone with a front northeast of Lake Baikal that transported the CO up
397 along the WCB (Figs. 7a and 8). Figure 5b shows that the relative humidity reached about
398 65 % in the MOZAIC measurement, suggesting the air mass indeed came from a WCB
399 (Cooper et al., 2002). The MOZAIC ozone profile also shows elevated ozone at the same
400 altitudes but the shape does not follow exactly the ones of CO and humidity, implying
401 complexity of chemical processes involved. The polluted air reached as high as 9 km
402 although most particles remained at heights of about 3-8 km (Fig. 8). After being lifted to
403 higher altitudes, the polluted air was transported by strong westerlies over long distances.
404 Figure 8 shows that the particles were further transported to the east and sink slowly after
405 7 June. Around 14 June 2003, the particles reached the east coast of Canada (0-5 km).
406 The satellite MODIS data show a large number of hot spots near Lake Baikal in May and
407 June 2003. Earlier studies have shown that forest fires in Asia can impact air quality in
408 North America (Jaffe et al., 2004; Liang et al., 2004; Oltmans et al., 2010). This case
409 illustrates again the role that WCBs played in the intercontinental transport of pollution
410 for such high CO. Notice that the FLEXPART simulation was made by using the FNL
411 meteorological data, which may have not considered the buoyancy force due to fires.
412 Such buoyancy force can lift CO plumes even faster and higher.

413 Our analyses are consistent with Nédélec et al. (2005), who examined 320 MOZAIC
414 flight routes from Europe to Asia in 2003 and reported the observations of high CO up to
415 800 ppbv above 8 km (~ 350 hPa) on 3 and 4 June 2003 around 57 °N (northeast of Lake

Baikal). With different data sets, i.e., Along Track Scanning Radiometer (ATSR) fire data, the Total Ozone Mapping Spectrometer (TOMS) aerosols data, and the MODIS cloud data, Nédélec et al. (2005) also attributed the high CO at these altitudes to front lifting of CO from large forest fires near Lake Baikal. The time and location of frontal lifting of CO in our FLEXPART simulations match well with the observations of high CO by Nédélec et al. (2005). Furthermore, this study provides a more explicit description on the CO transport pathways (Figs. 7 and 8). We also found this rare case demonstrate MOPITT's capability of detecting extreme high CO episodes through relative variations in vertical and horizontal dimensions. Corresponding to the strongest CO source among the three cases, MOPITT data showed the largest horizontal area with CO plumes (Fig. 4), the deepest vertical CO buildup with the highest abundances (Fig. 6), and the biggest enhancement of 200-250 ppbv from the a priori (Fig. 5).

4.2 Case study II: 18 March 2004

This case occurred on 18 March 2004 when high CO appeared in the MOPITT data in the lower and middle troposphere over the East China Sea (Fig. 4b). The elevated CO of 200-250 ppbv is observed between 750 and 550 hPa vertically in MOPITT data (Fig. 5c). The departure of the MOPITT CO profile from its a priori reflects the MOPITT's vertical sensitivity (Fig. 5c). The MOPITT monthly mean, like for the other two cases, follows a typical CO profile pattern with CO concentrations being the highest near the surface and decreasing gradually with altitude. The CO on 18 March 2004 was 50 ppbv higher than the monthly mean above 800 hPa. A layer of elevated CO appeared in the MOZAIC profile between 750-550 hPa with a peak of 500 ppbv around 650 hPa (Fig. 5d).

The high RH (~ 90-100 %) below 600 hPa in the MOZAIC data suggests that the air mass experienced some uplifting process that enhanced its humidity, likely from a WCB. The MOZAIC ozone peaked (~ 70 ppbv) around the same altitudes as CO, implying that ozone may be produced in the air mass carrying high CO during the transport process. Figure 6b shows a latitude-altitude cross section averaged between the two blue dashed lines in Fig. 4b. Around 30 °N, elevated CO levels (~ 200 ppbv) are evident around 700 hPa.

This case was simulated with GEOS-Chem to identify the sources of CO and to explore the transport mechanisms. The MODIS fire data suggest biomass burning over northern Indochina peninsula to be a source for the observed high CO (Fig. 9). The time series of fire counts over area of 20-25 °N and 92-105 °E peaked on 12 March 2004. Correspondingly, high CO of ~ 300 ppbv appeared in the MOPITT composite of 11-18 March 2004 at 700 hPa over northern Indochina peninsula (Fig. 9). This source was also recognized in the GEOS-Chem simulation (Fig. 10b). In addition, the anthropogenic source concentrated over the North China Plain (approximately 30-40 °N, 110-125 °E) was identified as another source (Fig. 10c). The fire-induced CO spread larger areas from south to north than the anthropogenic CO. Figure 11 shows the latitude-altitude cross sections of the GEOS-Chem simulations of CO, fire-induced CO, and anthropogenic CO, respectively, along 130 °E on 18 March 2004. CO abundances from both sources were high around 700 hPa (Figs. 11b and 11c) between 25-35 °N across 130 °E where MOPITT also observed high CO (Fig. 6b).

The different CO distributions for the two sources in three dimensions (Figs. 10 and 11) reflect rather different transport pathways and uplifting mechanisms. We found that

462 the transport of the fire-induced CO can be divided into four processes. First, the CO was
463 orographically lifted along the Hengduan Mountains from the surface to ~ 750 hPa. The
464 lifted CO is shown in Fig. 12 around 100 °E on a longitude-altitude cross section along
465 22 °N. Then, the uplifted CO experienced two separate transports. In the second process,
466 part of the lifted CO was further transported upward to 400-300 hPa, shown as a bulb in
467 Fig. 12 around 105 °E. This is due to strong convection, possibly caused by a frontal
468 system developed on 17 March 2004 (Fig. 9), interplayed with the leeside troughs east of
469 the Hengduan Mountains. The vertical velocity reached 0.2 m s^{-1} in FNL data around this
470 level (not shown). The ECMWF (European Centre for Medium-Range Weather Forecasts)
471 data also show northeastward airflow from Indochina peninsula with high potential
472 energy (warm and wet) available for strong convection. All of these suggest that the
473 strong convection over the leeside troughs rapidly lifted CO up to ~350 hPa. In fact, the
474 orographic lifting and topography-induced convection are quite common in this region so
475 high CO often appears at these two altitudinal levels in March as simulated by
476 GEOS-Chem (not shown). On 17 March, the lifted CO was with even higher
477 concentrations (~ 500 ppbv) around 400 hPa than the monthly mean because of its fire
478 origin and presence of the leeside troughs. In the third process, the uplifted CO around
479 400-300 hPa (near 105 °E in Fig. 12) was transported northeastward by strong winds
480 along the front in the upper troposphere, reaching the East China Sea (near 30 °N, 130 °E)
481 on 18 March (Fig. 11b). This transport enables high CO from forest fires in southern Asia
482 in low latitudes to rapidly reach the upper troposphere in the mid-latitudes. In the fourth
483 process, paralleling to the second and third, part of the orographically uplifted CO was
484 afloat around ~700 hPa because of leeside-trough induced convection. This CO was

transported eastward along the isobars of the low pressure system around 700 hPa (Figs. 10 and 12). This process occurred at lower altitudes than processes two and three. The transport was slower and it took longer time (from 15 to 18 March) for the CO to reach the East China Sea. Processes two and three brought CO to the upper troposphere (200-300 hPa in Fig. 11b), while process four increased CO in the lower to middle troposphere (700-500 hPa in Fig. 11b). For the anthropogenic CO from the North China Plain, the vertical transport was mainly carried out by frontal lifting on 17 March 2004 (Fig. 9) and then the uplifted CO was transported eastward along 30 °N (Fig. 10c). Consequently, the total CO shows a buildup centered near 700 hPa around 30 °N and 130 ° E, mostly coming from the two CO sources (Figs. 11a-11c).

The Hengduan Mountains run mainly north to south, with elevations ranging from 1300 to 6000 metres. This topography provides a favorable condition for the formation of the leeside troughs if meteorology is satisfied. Such troughs promote vertical transport of CO on the east side of the Mountains (in the second and fourth processes), while the orographic lifting occurred on the west side of the Mountains (in the first process). The leeside troughs occur most and least frequently in spring and summer, respectively. Interannual variation of the leeside troughs is also observed.

Comparison of the vertical CO distributions between MOPITT and GEOS-Chem (Fig. 6b vs Fig. 11a) suggests that MOPITT can generally capture vertical transport of CO from forest fires and anthropogenic sources, although the magnitude of CO in MOPITT data was lower and there were also substantial gaps in the MOPITT images due to convective clouds. In the MOPITT data, high CO of ~ 200 ppbv reached up to 200 hPa. In the lower to middle troposphere, elevated CO (~ 200 ppbv) was centered around

650-700 hPa. These features are similar to the GEOS-Chem simulations. Note that the CO buildup around 300 hPa in the GEOS-Chem simulation (Figs. 11a and 11b) was reflected in the MOPITT data (Fig. 6b), but not as obvious as in the simulation since the MOPITT retrievals are smoothed with the averaging kernels. This CO is also shown as a little bump around 300 hPa in MOPITT vertical profile in Fig. 5c. This buildup is missing in the MOZAIC profile (Fig. 5d) because the aircraft flew towards the north and outside the region with high CO (Fig. 4b).

As the backward trajectories starting from the boxed area at 700 hPa in Figure 4b indicated the most particles came from the large fire in the Indochina peninsula starting from 11 March 2004, we released air particles in FLEXPART over the fire regions from the surface to 1 km on 11 March 2004, and forward trajectories were simulated to track down the air parcels until 18 May 2004 at 2 a.m. Taking the same zonal means as for Fig. 6b, it is found that the vertical distribution of particle concentrations is similar to that in Fig. 6b with highest particle concentrations between 4-5 km (not show). As simulated by FLEXPART, the outflow of the high CO finally reached the west coast of the United States with particles mainly distributed around 5 km in altitude. High CO observed in East Asia in this case appeared the most southerly among the three (Fig. 6), leading to a most southerly outflow.

The strong leeside-trough-induced convection described in the fourth process was first proposed by Lin et al. (2009) who found that the leeside troughs above the Indochina peninsula play a significant role in uplifting ozone there. In this study, we found these leeside troughs can promote lifting of CO even up to the upper troposphere (in the second process, Fig. 12). It is the interplay of the leeside troughs and the cyclone in the northeast

of China which formed a front system that transported CO from the Indochina peninsula upward.

4.3 Case study III: 10 April 2005

In this case, MOPITT observed high CO of ~ 250 ppbv at 300 hPa near the east coast of Japan on 10 April 2005 (Fig. 4c). Like for the other cases, the mean MOPITT profile was taken over a boxed area (in Fig. 4c) upwind of the MOZAIC measurement for comparison. The MOPITT vertical profile clearly shows a CO peak around 300 hPa, where it departs from the MOPITT monthly mean (Fig. 5e). Comparing with the other cases, MOPITT CO peaked at higher altitudes, illustrating some MOPITT vertical sensitivity even at these altitudes. In Fig. 5f, a sharp peak of 300 ppbv in MOZAIC CO is shown around 350 hPa. This peak can also be reproduced in the GEOS-Chem simulation with a lower CO abundance of ~200 ppbv (not shown). The profile of relative humidity follows closely that of CO, with values up to 90-100 % around 350 hPa, implying that the elevated CO was lifted to this level from the lower troposphere by a cyclone system along its WCB. However, the MOZAIC ozone profile varies differently from the CO profile. We found this is connected to a strong stratospheric intrusion introduced by the cyclone. HYSPLIT simulations suggest that a large amount of air mass plunged around 4 April from 9 to 3-4 km over northwest of China, bringing high ozone to the lower troposphere (not shown). Another piece of evidence for a stratospheric intrusion is suggested by the low humidity between 780-400 hPa. Such a downwelling of stratospheric air on the back side of cyclones was also reported by Miyazaki et al. (2003). Figure 6c shows an altitude-latitude cross section averaged between 120-150 °E (between two dashed lines in

554 Fig. 4c). High CO of 200-250 ppbv appeared between 300-200 hPa around 35 °N. This is
555 a rare case in which MOPITT reports such high CO (200-250 ppbv) at these high
556 altitudes (around 300 hPa). Documented CO abundances observed by MOPITT at these
557 altitudes were ~130 ppbv over Indian summer monsoon seasons (Kar et al., 2004),
558 110-150 ppbv in the North America from the forest fires, chemical, and anthropogenic
559 sources (Liu et al., 2005; 2006), and ~150 ppbv in spring at Hong Kong (Zhou et al.,
560 2013).

561 The MODIS fire data show that there were indeed large fires over Indochina
562 peninsula in 3-10 April 2005, shown as stars in Fig. 13. Using GEOS-Chem, CO from
563 fire and anthropogenic sources was simulated to identify their respective contributions
564 and transport pathways.

565 The entire process of vertical and horizontal transport of CO was well reproduced by
566 GEOS-Chem (Fig. 14). Figure 14a provides the CO distribution in the lower troposphere
567 on 8 April 2005, while Figs. 14b and 14c show the CO distribution on the next day and
568 the day after in the middle and upper troposphere, respectively. The geopotential heights
569 at 750, 450, and 250 hPa are overlaid with the CO images for each layer accordingly. On
570 8 April 2005, there was a cyclone developing in the east of Lake Baikal between 110-120 °
571 E, 45-55 °N. The surface CO was transported upward and northeastward along the WCB
572 (Fig. 14a). On April 9, the cyclone moved to the east (Figs. 13 and 14b). The high CO
573 shows a "comma" shape along WCB at the mid-troposphere; this shape is typical for a
574 mature cyclone system with a WCB (Cooper et al., 2002). On April 10, the cyclone
575 further moved eastward and reached the Sea of Japan (Fig. 14c). The GEOS-Chem
576 simulation shows accumulation of high CO over the ridge of high pressure and along the

front at the upper troposphere. The GEOS-Chem simulations suggest that the outflow of the high CO reached Canada on April 16.

The combined effects of cyclone activities, topography, and CO from different sources and locations are reflected in distinct CO signatures along the WCB. Figure 15 shows the CO from the fires (Figs. 15a and 15c) and from the anthropogenic source (Figs. 15b and 15d) in the middle and upper troposphere, respectively, overlaid with the geopotential height at 450 hPa (Figs. 15a and 15b) and 250 hPa (Figs. 15c and 15d), respectively. In the middle troposphere (500-400 hPa), a large amount of CO from the fires in Indochina peninsula was uplifted to this level through orographic lifting and strong convection on the west and east side of the Hengduan Mountains, respectively. This CO distributed along the middle part of the WCB on 9 April 2005 and was transported eastward on 10 April 2005 (Fig. 15a). One source of the anthropogenic CO was concentrated around the North China Plain (Ding et al., 2009) where high CO was evident in MOPITT data (Fig. 13, 35-45 °N, 100-120 °E). On April 8, this CO was uplifted along the WCB and further transported to the middle troposphere, coming across sudden elevated terrains on the way and forming the head of the "comma" in the cyclone system (Figs. 14b and 15b). The topography's role was noticed by Liu et al. (2003), who found a ring of convergence around the North China Plain associated with elevated terrain, and by Ding et al. (2009), who speculated possible topography lifting in the North China Plain. In the southern end of the WCB (near 30 °N, 120 °E in Fig. 15b), the CO came from the anthropogenic source in the vicinity of the Sichuan basin (~ 26-34 °N, 102-110 °E). This CO was transported vertically to 500 hPa on April 8 at 18:00 UTC to April 9 at 00:00 UTC. Air pollution often accumulates in the Sichuan basin because of its

special topography. The development of small scale cyclones there is well known as the southwest vortex or Sichuan low (Tao and Ding, 1981). Accumulated pollutants there usually are transported to the free troposphere by such convection. The strong convection can last more than 6 h and peak at the midnight (Yu et al., 2007). As this anthropogenic source is quite stable, its contribution should not be understated.

Interestingly, Lin et al. (2009) reported an observed ozone enhancement from ozonesonde data at 4 km in Taiwan on 11 April 2005. They proposed a new transport mechanism from their study as discussed in Sect. 4.2, in which they attributed the elevated ozone to the biomass burning in Indochina. Similarly, CO from biomass burning was also apparent over Taiwan at the middle troposphere in the GEOS-Chem simulation (Fig. 15a), although the maximum CO enhancement was north of Taiwan at this altitude.

The white dot in Fig. 15 indicates the location where MOZAIC passed over. It is clear that MOZAIC measurement at 200-300 hPa was within the WCB, while it was at a distance from the WCB at 500-400 hPa. This is consistent with the MOZAIC CO, ozone, RH profiles shown in Fig. 5f, suggesting that MOZAIC in fact measured air from the stratosphere at these altitudes. As the wind was stronger in the upper than in the lower troposphere, the WCB-transported CO reached further east in the upper levels (Fig. 15). The simulations suggest that over the boxed area in the MOPITT image in Fig. 4c at 300 hPa, the fire and anthropogenic sources contributed approximately 15% and 20 % CO, respectively. It is noteworthy that there were large gaps in MOPITT data north of 33 °N (Fig. 4c) where CO abundances may be even higher than the MOPITT CO south of 33 °N as suggested by the GEOS-Chem simulation (Fig. 14c). These gaps were caused by clouds associated with the cyclone system. The complication due to clouds is a problem

623 with an optical instrument like MOPITT. This is why this care is rare which high CO was
624 observed by both MOPITT and MOZAIC under a frontal system.
625 In this case, the strong part of the front (close to the centre of the cyclones) swept
626 southern China, where CO was high (Fig. 13). Along the front (30-40 °N, 100-120 °E),
627 the temperature gradient at 925 hPa was as high as 4.9 C per degree. Strong ascents
628 occurred ahead of the front, with vertical velocity being ~ 0.05 m s^{-1} at 900 hPa and ~
629 0.20 m s^{-1} at 750 hPa, increasing with altitude until 300-250 hPa where the maximum
630 vertical velocity was 0.26 m s^{-1}. Consequently, the high CO can be rapidly lifted to the
631 upper troposphere in this case.
632 FLEXPART was also used to trace down high CO in the MOPITT image by releasing
633 air particles in the boxed area in Fig. 6c (indicated by a bar in Fig. 4c). We found that the
634 most CO came from the southwest part of China (boxed area in Fig. 13) where MOPITT
635 CO composite of 3-10 April 2005 shows high CO of 250-300 ppbv. This CO was lifted
636 along the WCB described above. This agrees with the GEOS-Chem simulation which
637 attributed the major CO source in the upper troposphere to the anthropogenic CO, likely
638 from the Sichuan Basin (Fig. 15d).
639

640 # 5 Discussion

641 New insights gained from this study and suggestions for future work are discussed as
642 follows.

643 ## 5.1 Observations of high CO episodes

644 In the three CO episodes, high CO abundances 300-550 ppbv were observed by
645 MOZAIC in the free troposphere (Fig. 5). The CO abundances are among the highest

documented at these altitudes in East Asia. Ding et al. (2009) observed high CO episode of ~1185 ppbv at 2.6 km (850-700 hPa) over the North China Plain in summer 2007. Nédélec et al. (2005) found CO up to 800 ppbv above 8 km (~400 hPa) near the fire region of Lake Baikal on 3 and 4 June 2003. Highest CO concentrations during TRACE-P were between 250-300 ppbv from 2 to12 km (Heald et al., 2003; Liu et al., 2003; Miyazaki et al., 2003). Occurrences of such high CO episodes are not by chance. They reflect the uniqueness and complexity of meteorology, orography, vegetation covers, and CO sources in East Asia. For example, in all the cases, biomass burning occurred from regions with dense vegetation covers and with most active forest fires in East Asia (Schultz, 2002; Duncan et al., 2003). These fires are usually most active in summer in boreal forest in Russia, like in case 2003, and in spring in the southern East Asia, like cases 2004 and 2005, thus enhancing chances of high CO episodes in these seasons.

The frequency of occurrences of such high CO is illustrated in Table 2. As the three cases occurred near Japan, MOZAIC data around the vicinity of Narita from 2001 to 2006 are summarized, showing occurrences of various CO abundance ranges in the boundary layer (the surface-850 hPa), the lower (850-600 hPa), middle (600-400 hPa), and upper (400-200 hPa) troposphere. Among all the data in the upper troposphere, CO abundances occurred 93 times (17%) between 200-300 ppbv, 19 times (4%) between 300-400 ppbv, and 6 times (1%) over 400 ppbv. In the middle troposphere, the fraction of occurrences of CO within 200-300, 300-400, and over 400 ppbv was 14%, 3%, and 2%, respectively. In the boundary layer, the highest occurrences of CO abundances (38% of all the data in the layer) were within a range of 200-300 ppbv, while the range was within 100-200 ppbv in the lower (47%), middle (74%), and upper troposphere (66%).

669 Seasonally, there were more high CO episodes in the higher altitudes in spring and
670 summer than in fall and winter.
671 The frequency of such high CO episodes is also examined in the GEOS-Chem
672 simulations and MOPITT observations in the vicinity of Narita (126-140 °E, 30-40 °N) in
673 2005 (Table 3). A count is added to a CO range if the daily maximum CO in the area
674 (126-140 °E, 30-40 °N) falls into that CO range. Thus, the total counts for all the CO
675 ranges at a given layer are 365 in 2005 for GEOS-Chem, while the counts are 281 for
676 MOPITT due to missing data. To minimize noise in daily MOPITT data, only when there
677 are at least 10 data with the maximum CO falling into a given CO range, a count is added.
678 GEOS-Chem can simulate CO up to 400 ppbv in the upper troposphere, while the
679 maximum CO in MOPITT is lower so that different CO ranges are used in Table 3.
680 Overall, MOZAIC, MOPITT and GEOS-Chem all show a high frequency of high CO
681 (larger than 200 ppbv) at the surface, progressively shifting to a high frequency of low
682 CO (less than 200 ppbv) at the upper troposphere. Between 400-200 hPa, CO with
683 200-300 ppbv occurred 1.2 times every 10 days in GEOS-Chem, which was slightly
684 lower than in MOPITT (1.8 times) and MOZAIC (1.7 times). Overall, MOZAIC
685 observed 2-5% more vertical transport of high CO (>300 ppbv) to the upper troposphere
686 than GEOS-Chem, while the latter simulated 10-20% more frequently the transport to the
687 middle and lower troposphere with similar or lower CO abundances.
688 It is likely that on average, the extremely high CO episodes (~500 ppbv), such as the
689 2003 and 2004 cases (Fig. 5), occurred 2-5 times per 100 days in their respective altitudes
690 over the East China Sea and the Sea of Japan (Tables 2 and 3). With a lower CO
691 abundances of 200-300 ppbv (case 2005), the frequency for the air mass to be transported

to 400-200 hPa is1-2 times per 10 days (Tables 2 and 3). The frequency can be even higher in spring and summer, approximately once a week (Table 2). Significant impacts of such vertical transport can be expected on the air quality downwind and climate on the global climate. The transport mechanisms and CO source contributions revealed in this study can also be applicable for CO episodes with lower CO abundances or at lower altitudes.

5.2 The role of topography

East Asia's topography varies significantly across its vast width, increasing from east to west, with a variety of terrains. This study found that topography there affected the three cases in different ways. In addition to its general function in orographic lifting (in cases 2004 and 2005), topography also interplay with frontal systems and enhance the uplifting substantially in the North China Plain (in cases 2004 and 2005). It is notable that CO transports from south to north along elevated terrain over China (in case 2005, Fig. 14a). Under the influence of the Tibetan Plateau, the southwest vortex (or the Sichuan low) is formed (Tao and Ding, 1981) and can facilitate strong convection in the Sichuan basin (in case 2005).

In particular, topography-induced convection due to the leeside troughs east of the Hengduan Mountains, proposed by Lin et al. (2009), offers a new mechanism for vertical transport of pollutions from the region (in cases 2004 and 2005). Lin et al. (2009) mainly aimed at pollution transport to the lower and middle troposphere. Extending from Lin et al. (2009), this study found such a mechanism to be plausible in explaining pollution transport to the upper troposphere. We found that the impacts of the topography-induced

715 convection on vertical CO transport vary substantially from year to year. A study on such
716 interannual variation is underway.
717
718 ## 5.3 The implications of WCB trends on uplifting of CO
719 Extratropical cyclones and associated frontal activities are important in lifting CO
720 from the boundary layer to the free troposphere. This also applies to other air pollutants.
721 Zhao et al. (2008) found that the influence of Asian dust storms on North American
722 ambient particulate matter levels is highly related to the height to which the frontal
723 cyclones in East Asia can lift dust. Although many functions and characteristics of WCBs
724 have been recognized by earlier studies, we found some details new or unique for the
725 three cases. In case 2004, it is the interplay of the leeside troughs and the cyclone in the
726 northeast of China that transported CO from the Indochina peninsula upward. The high
727 CO in this case appeared the most southerly among the three, leading to a most southerly
728 outflow. In case 2005, the downwelling of stratospheric air on the back side of cyclones
729 was recognized. The CO along various parts of the WCB was identified to be of fire
730 origin from Indochina and anthropogenic origin from Sichuan and the North China Plain.
731 The source allocation was sensitive to the location of the front. Comparing cases 2004
732 and 2005, we found that uplifting of CO to the upper troposphere became possible when
733 large CO sources coincided with the strongest part of a WCB.
734 In East Asia, cyclones occur most frequently in two regions in spring and summer:
735 one over the lee sides of the Altai-Sayan and the other in the East China Sea and the Sea
736 of Japan (Chen et al., 1991; Yue and Wang, 2008). These are the locations and seasons
737 where and when we can expect similar events to happen in the future. Chen et al. (1991)

suggested a decline in cyclonic events in East Asia from 1957 to 1977 and no such decline from 1977 to 1987. Recently, an analysis for a longer term from 1951 to 2010 based on ensembles of Twentieth Century Reanalysis (20CR) showed a decreasing trend in the northern part of the Sea of Japan and an increasing trend over the southern part of the Sea of Japan and the leeside of the Altai-Sayan in summer (Wang et al., 2013). The implications of these trends on uplifting of CO deserve further investigation. It would be helpful to conduct statistical analysis of the CO source distribution along WCBs in East Asia in the future.

5.4 Model simulations of pollution transport

Pollution transport can be tracked computationally with Eulerian and Lagrangian approaches, as represented by GEOS-Chem and FLEXPART models, respectively. GEOS-Chem can not only track transport of CO (a physical process) but also consider chemical reactions during the transport while FLEXPART can visualize transport pathways and pin down source regions effectively, without considering chemical functions in the meantime. GEOS-Chem can also fill the gaps in MOPITT satellite data (Figs. 10, 11, and 14). We found that GEOS-Chem simulates the observed aircraft and satellite CO well in cases 2004 and 2005 but cannot fully reproduce the elevated CO in MOZAIC data in case 2003. The simulated CO plume is with lower mixing ratios and at lower altitudes than in the MOZAIC data. This is possibly due to an underestimated fire inventory or conservative parameterizations in simulating large forest fires or both in GEOS-Chem. Nassar et al. (2009) reported underestimated CO over the 2006 Indonesia fire region by GEOS-Chem, in comparison with the Tropospheric Emission Spectrometer

761 (TES) observations. FLEXPART can generally simulate the three cases, strikingly well
762 sometimes in agreement with observed details in space and time, although discrepancies
763 between FLEXPART and satellite and aircraft observations can be found in various
764 places on small scales. FLEXPART simulates strong sources well but omits weak sources
765 sometimes.
766

767 ## 5.5 Applications of MOPITT data

768 We analyzed MOPITT data from two aspects: vertical sensitivity on the synoptic
769 scale. Both are challenging and have not been studied adequately. Large gaps due to
770 clouds and the limited MOPITT swath make application of MOPITT on the synoptic
771 scale difficult. Thus application of MOPITT data over East Asia were mostly focused on
772 monthly or seasonal scales (Tanimoto et al., 2008; Zhao et al., 2010; Hao et al., 2011; Liu
773 et al., 2011; Zhou et al., 2013; Su et al., 2014). This study shows that even with large
774 gaps, daily MOPITT data can capture vertical disturbances of CO on the synoptic scale,
775 which are usually diluted on longer time scales. This study also suggests the importance
776 of filling the gaps with other satellite data or in designing new satellite instruments, for
777 the purpose of detecting such variation over large areas on the regional and global scales.
778 Typically for satellite remote sensing products, the MOPITT retrieval at a specific
779 pressure level is influenced by CO from other levels and thus its retrieval at that pressure
780 level can be biased. However, MOPITT can more accurately measure the average CO
781 mixing ratio over a thick layer, resulting in a coarse vertical resolution. It was suggested
782 that the vertical variation in CO cannot be fully resolved in earlier applications of
783 MOPITT data (Jacob et al., 2003). This study addressed the MOPITT vertical sensitivity

784 with newly MOPITT V5 data and found enhanced vertical sensitivity in V5 data in the
785 free troposphere, even in the upper troposphere, in addition to in the boundary layer
786 emphasized by Worden et al. (2010) and Deeter et al. (2012). The enhanced DFSs and the
787 averaging kernels in V5 illustrated by Worden et al., (2010) and Deeter et al. (2012) are
788 supported (Figs. 1 and 5 and Sect.3).

789 In Fig. 5, the smoothed MOZAIC profiles were calculated using the averaging
790 kernels and the a priori in an area upwind of the MOZAIC measurement within 0-10 °
791 distance for each case as there were no MOPITT data available at the exact locations of
792 the MOZAIC measurements. Although this may introduce some bias, the averaging
793 kernel smoothed MOZAIC profiles in V5 show more vertical structure in CO than an
794 earlier version of MOPITT data in Jacob et al. (2003, in their Fig. 4). Overall, this study
795 found: (1) MOPITT can differentiate the magnitude of CO plumes originated from strong
796 or weak sources (Figs. 4, 5, and 6), (2) MOPITT can distinguish elevated CO in the lower,
797 middle, and upper troposphere (Figs. 4, 5, and 6), (3) the shape of CO plumes in vertical
798 direction matches with simulations of GEOS-Chem and FLEXPART, sometimes
799 remarkably well (Figs. 6, 8, and 11), and (4) there is more vertical structure in CO in new
800 V5 than in earlier versions of MOPITT data (Fig. 5).

801 It is the relative variations in MOPITT CO data that help diagnose CO transport
802 vertically or horizontally. This study suggests using MOPITT data quantitatively with
803 caution, especially at altitudes with high CO plumes because, as illustrated in Figs. 5 and
804 6, the magnitude of elevated CO in the MOPITT data could be lower than that in the
805 MOZAIC data at the altitudes where CO peaked. Therefore, the vertical variation of CO,
806 even enhanced in V5, is still much smoothed in MOPITT data. MOPITT can distinguish

807 elevated CO in different layers of the free troposphere, yet sometimes cannot specify the
808 exact altitude of elevated CO shown in the MOZAIC measurements (Figs. 5 and 6). One
809 limitation for MOPITT's application of vertical transport is the complication of clouds,
810 which often accompany with frontal systems. As shown in cases 2004 and 2005, CO is
811 usually high in cloudy areas. Therefore, the magnitude of CO abundances can be
812 underestimated by MOPITT in these areas.
813
814 **6 Conclusions**
815 East Asia is characterized by its unique and complex meteorology, topography,
816 vegetation covers, and CO sources. The characteristics are reflected in uplifting of CO
817 illustrated in three high CO episodes during 2003-2005 in this study. Through integrated
818 analyses of observations from the airborne MOZAIC and spaceborne MOPITT
819 instruments and simulations from a trajectory dispersion model FLEXPART (Stohl et al.,
820 2005) and a chemical transport model GEOS-Chem (Bey et al., 2001), this study draws
821 the following conclusions.
822 1. In the three CO episodes, high CO abundances of 300-550 ppbv were observed by
823 MOZAIC in the free troposphere over the East China Sea and the Sea of Japan.
824 These are among the highest CO abundances ever documented at these altitudes.
825 The three cases occurred when and where meteorology was favorable and CO
826 sources were strong. It is likely that on average, the extremely high CO episodes
827 (~500 ppbv) like cases 2003 and 2004 occurred 2-5 times every 100 days in their
828 respective altitudes over the region, while in case 2005, episodes with a lower CO
829 abundances (200-300 ppbv) occurred 1-2 times per 10 days between 400-200 hPa.

CO episodes in even lower altitudes and with even lower abundance occurred more frequently in the region.

2. GEOS-Chem and FLEXPART simulations reveal different CO signatures from biomass burning and anthropogenic sources in the CO enhancement in the three cases, reflecting different transport pathways and mechanisms and locations of both sources. In case 2003, CO from large forest fires near Lake Baikal dominated the elevated CO. In case 2004, anthropogenic CO came from the North China Plain and mostly reached ~ 700 hPa near the East China Sea, while CO from biomass burning in Indochina was transported through two separate pathways, leading to two distinct CO enhancements around 700 hPa and 300 hPa. In case 2005, along a WCB over the East China Sea and the Sea of Japan, anthropogenic CO from the North China Plain and from the Sichuan basin prevailed in the northern and southern part of the WCB, while CO from biomass burning in Indochina was mostly distributed in the middle part of the WCB.
3. Topography in East Asia influences vertical transport of CO in different ways. In particular, topography-induced leeside troughs east of the Hengduan Mountains over Indochina lead to strong convection. This new mechanism proposed by Lin et al. (2009) is supported by this study in explaining CO transport to the middle troposphere and further extended for CO transport to the upper troposphere. Strong convection from the Sichuan basin also plays an important role in vertically transporting anthropogenic CO. The topography interacting with frontal activities can enhance the vertical transport of CO substantially in the North China Plain.
4. Extratropical cyclones and associated frontal activities are important mechanism in

lifting CO from the boundary layer to the free troposphere, as illustrated by the three cases and earlier studies. East Asia is one of two regions between 25-45 °N with most frequent WCB events (Eckhardt et al., 2004). Inside East Asia, there are two regions where cyclones occur most frequently: one over the lee sides of the Altai-Sayan and the other in the East China Sea and the Sea of Japan, occurring mostly in spring and summer over both regions (Chen et al., 1991). The seasons and locations of the three high CO episodes just match well with these two areas and active cyclone seasons, which may not happen by chance.

5. Biomass burning is identified as an important source for all three episodes, suggesting that CO from sporadic fire activities can provide additional CO to less varying anthropogenic emission and enhance chances of high CO episodes. The fire regions shown in this study are the places with dense vegetation covers and with most active forest fires in East Asia.
6. The MOPITT's vertical sensitivity is found to be enhanced in its new V5 NIR/TIR data in the free troposphere, even in the upper troposphere. The daytime V5 data can detect synoptic disturbances of weather systems on horizontal variation of CO. The data also show more vertical structure than earlier versions and can distinguish CO enhancements at different layers of the troposphere, although the detected high CO is over a broad range in altitudes and lacks detailed vertical structure in comparison with the aircraft observations. Because the CO retrieval at a certain pressure level is often smoothed by the MOPITT averaging kernels, the MOPITT retrievals usually underestimate elevated CO at altitudes with peak CO plumes. The complication of clouds within frontal systems can generate large gaps in

MOPITT data and cause underestimation of CO statistically in these regions. Nevertheless, MOPITT data can be used to qualitatively help diagnose vertical transport processes, with caution on their absolute CO values. On average, MOPITT slightly overestimates the background CO in the upper troposphere.

Acknowledgements.

The authors gratefully acknowledge the following data and modeling tools. The satellite CO data are provided by the MOPITT team and acquired from the NASA Langley Research Center Atmospheric Science Data Center. The MOZAIC CO data are from the European Commission, Airbus, and the Airlines (Lufthansa, Austrian, Air France) who carry free of charge the MOZAIC equipment and perform the maintenance since 1994. The Final Analysis Data (FNL) were obtained from NOAA CDC. The GEOE-Chem model is developed and managed by the Atmospheric Chemistry Modeling Group at Harvard University with support from the NASA Atmospheric Chemistry Modeling and Analysis Program (ACMAP). The FLEXPART model development team consists of Andreas Stohl, Sabine Eckhardt, Harald Sodemann, and John Burkhart at the Norwegian Institute for Air Research (NILU). Insights and critiques from two anonymous reviewers are highly appreciated. Financial support is provided by an open fund from the Institute of Remote Sensing and Digital Earth, Chinese Academy of Sciences (OFSLRSS201107), the Key Basic Research Program (2010CB950704, 2014CB441203), and the Natural Science Foundation of China (41375140).

References

Banic, C. M., Isaac, G. A., Cho, H. R., and Iribane, J. V.: The distribution of pollutants near a frontal surface: a comparison between field experiment and modeling, Water Air Soil Poll., 30, 171-177, 1986.

Barret, B., Le Flochmoen, E., Sauvage, B., Pavelin, E., Matricardi, M., and Cammas, J. P.: The detection of post-monsoon tropospheric ozone variability over south Asia using IASI data, Atmos. Chem. Phys., 11, 9533-9548, doi:10.5194/acp-11-9533-2011, 2011.

Berntsen, T. K., Karlsdóttir, S., and Jaffe, D. A.: Influence of Asian emissions on the composition of air reaching the north western United States, Geophys. Res. Lett., 26, 2171-2174, doi:10.1029/1999GL900477, 1999.

Bertschi, I. B., Jaffe, D. A., Jaeglé, L., Price, H. U., and Dennison, J. B.: PHOBEA/ITCT 2002 airborne observations of trans-Pacific transport of ozone, CO, VOCs and aerosols to the northeast Pacific: impacts of Asian anthropogenic and Siberian Boreal fire emissions, J. Geophys. Res., 109, D23S12, doi:10.1029/2003JD004328, 2004.

Bethan, S., Vaughan, G., Gerbig, C., Volz-Thoms, A., Richer, H., and Tiddeman, D. A.: Chemical air mass differences near fronts, J. Geophys. Res., 103, 13413-13434, 1998.

Bey, I., Jacob, D. J., Yantosca, R. M., Logan, J. A., Field, B. D., Fiore, A. M., Li, Q., Liu, H. Y., Mickley, L. J., and Schultz, M. G.: Global modeling of tropospheric chemistry with assimilated meteorology: model description and evaluation, J. Geophys. Res., 106, 23073-23095, 2001.

Brown, R. M., Daum, P. H., Schwartz, S. E., and Hjelmfelt, M. R.: Variations in the chemical composition of clouds during frontal passage, in: The Meteorology of Acid Deposition, edited by: Samson, P. J., Air Pollut. Control Assoc., Pittsburgh, Pa., 202-212, 1984.

Chan, D., Yuen, C. W., Higuchi, K., Shashkov, A., Liu, J., Chen, J., and Worthy, D.: On the CO_2 exchange between the atmosphere and the biosphere: the role of synoptic and mesoscale processes, Tellus B, 56, 194-212, 2004.

Chen, B., Xu, X. D., Yang, S., and Zhao, T. L.: Climatological perspectives of air transport from atmospheric boundary layer to tropopause layer over Asian monsoon regions during boreal summer inferred from Lagrangian approach, Atmos. Chem. Phys., 12, 5827-5839, doi:10.5194/acp-12-5827-2012, 2012.

Chen, S., Kuo, Y., Zhong, P., and Bai, Q.: Synoptic climatology of cyclogenesis over East Asia, 1958-1987, Mon. Weather Rev., 119, 1407-1418, 1991.

Chung, K. K., Chan, J. C. L., Ng, C. N., Lam, K. S., and Wang, T.: Synoptic conditions associated with high carbon monoxide episodes at coastal station in Hong Kong, Atmos. Environ., 33, 3099-3095, 1999.

Cooper, O. R., Moody, J. L., Parrish, D. D., Trainer, M., Ryerson, T. B., Holloway, J. S., Hübler, G., Fehsenfeld, F. C., and Evans, M. J.: Trace gas composition of midlatitude cyclones over the western North Atlantic Ocean: a conceptual model, J. Geophys. Res., 107, D7, doi:10.1029/2001JD000901, 2002.

Cooper, O. R., Forster, C., Parrish, D., Dunlea, E., Habler, G., Fehsenfeld, F., Holloway, J., Oltmans, S., Johnson, B.,Wimmers, A., and Horowitz, L.: On the life-cycle of a stratospheric intrusion and its dispersion into polluted warm conveyor belts, J. Geophys. Res., 109, D23S09, doi:10.1029/2003JD004006, 2004.

Cooper, O. R., Stohl, A., Hubler, G., Hsie, E. Y., Parrish, D. D., Tuck, A. F., Kiladis, G. N., Oltmans, S. J., Johnson, B. J., Shapiro, M., Moody, J. L., and Lefohn, A. S.: Direct transport of midlatitude stratospheric ozone into the lower troposphere and marine boundary layer of the tropical Pacific Ocean, J. Geophys. Res., 110, D23310, doi: 10.1029/2005JD005783, 2005.

Cooper, O. R., Stohl, A., Trainer, M., Thompson, A., Witte, J. C., Oltmans, S. J., Johnson, B. J., Merrill, J., Moody, J. L., Tarasick, D., Nédélec, P., Forbes, G., Newchurch, M. J., Schmidlin, F. J., Johnson, B. J., Turquety, S., Baughcum, S. L., Ren, X., Fehsenfeld, F. C., Meagher, J. F., Spichtinger, N., Brown, C. C., McKeen, S. A., McDermid, I. S., and Leblanc, T.: Large upper tropospheric ozone enhancements above mid-latitude North America during summer: in situ evidence from the IONS and MOZAIC ozone monitoring network, J. Geophys. Res., 111, D24S05, doi:10.1029/2006JD007306, 2006.

Cristofanelli, P., Bonasoni, P., Collins, W., Feichter, J., Forster, C., James, P., Kentarchos, A., Kubik, P. W., Land, C., Meloen, J., Roelofs, G. J., Siegmund, P., Sprenger, M., Schnabel, C., Stohl, A., Tobler, L., Tositti, L., Trickl, T., and Zanis, P.: Stratosphere-to-troposphere transport: a model and method evaluation, STACCATO special section of J. Geophys. Res., 108, 8525, doi:10.1029/2002JD002600, 2003.

Daley, R.: Atmospheric Data Analysis, Cambridge University Press, Cambridge, 1991.

Damoah, R., Spichtinger, N., Forster, C., James, P., Mattis, I., Wandinger, U., Beirle, S., Wagner, T., and Stohl, A.: Around the world in 17 days - hemispheric-scale transport of forest fire smoke from Russia in May 2003, Atmos. Chem. Phys., 4, 1311-1321, doi:10.5194/acp-4-1311-2004, 2004.

Davies, D. K., Ilavajhala, S., Wong, M. M., and Justice, C. O.: Fire information for resource management system: archiving and distributing MODIS active fire data, IEEE T. Geosci. Remote, 47,72-79, 2009.

Deeter, M. N., Emmons, L. K., Francis, G. L., Edwards, D. P., Gille, J. C., Warner, J. X., Khattatov, B., Ziskin, D., Lamarque, J.-F., Ho, S.-P., Yudin, V., Attié, J.-L., Packman, D., Chen, J., Mao, D., and Drummond, J. R.: Operational carbon monoxide retrieval algorithm and selected results for the MOPITT instrument, J. Geophys. Res., 108, 4399, doi:10.1029/2002JD003186, 2003.

Deeter, M. N., Emmons, L. K., Edwards, D. P., Gille, J. C., and Drummond, J. R.: Vertical resolution and information content of CO profiles retrieved by MOPITT, Geophys. Res. Lett., 31, L15112, doi:10.1029/2004GL020235, 2004.

Deeter, M. N., Worden, H. M., Edwards, D. P., Gille, J. C., and Andrews, A. E.: Evaluation of MOPITT retrievals of lower-tropospheric carbon monoxide over the United States, J. Geophys. Res., 117, D13306, doi:10.1029/2012JD017553, 2012.

Deeter, M. N., Mart ́nez-Alonso, S., Edwards, D. P., Emmons, L. K., Gille, J. C., Worden, H. M., Pittman, J. V., Daube, B. C., and Wofsy, S. C.: Validation of MOPITT Version 5 thermal-infrared, near-infrared, and multispectral carbon monoxide profile retrievals for 2000–2011, J. Geophys. Res., doi:10.1002/jgrd.50272, 2013.

Dickerson, R. R., Huffman, G. J., Luke, W. T., Nunnermacker, L. J., Pickering, K. E., Leslie, A. C. D., Lindsey, C. G., Slinn, W. G. N., Kelly, T. J., Daum, P. H., Delany, A. C., Greenberg, J. P., Zimmerman, P. R., Boatman, J. F., Ray, J. D., and Stedman, D. H.: Thunderstorms – an important mechanism in the transport of air pollutants, Science, 235, 4787, 460-464, 1987.

Dickerson, R. R., Li, C., Li, Z., Marufu, L., T., Stehr, J. W., McClure, B., Krotkov, N., Chen, H., Wang, P., Xia, X., Ban, X., Gong, F., Yuan, J., and Yang, J.: Aircraft observations of dust and pollutants over northeast China: insight into the meteorological mechanisms of transport, J. Geophys. Res., 112, D24S90, doi:10.1029/2007JD008999, 2007.

Ding, A., Wang, T., Xue, L., Gao, J., Stohl, A., Lei, H., Jin, D., Ren, Y., Wang, X., Wei, X., Qi, Y., Liu, J., and Zhang, X.: Transport of north China air pollution by midlatitude cyclones: case study of aircraft measurements in summer 2007, J. Geophys. Res., 114, D08304, doi:10.1029/2008JD011023, 2009.

Donnell, E. A., Fish, D. J., Dicks, E. M., and Thorpe, A. J.: Mechanisms for pollutant transport between the boundary layer and the free troposphere, J. Geophys. Res., 106, 7847-7856, 2001.

Drummond, J. R.: Measurements of pollution in the troposphere (MOPITT), in: The Use of EOS for Studies of Atmospheric Physics, edited by: Gille, J. C. and Visconti, G., North Holland, New York, 77-101, 1992.

Drummond, J. R. and Mand, G. S.: The measurements of pollution in the troposphere (MOPITT) instrument: overall performance and calibration requirements, J. Atmos. Ocean. Tech., 13, 314-320,
1996.

Duncan, B. N., Martin, R. V., Staudt, A. C., Yevich, R., and Logan, J. A.: Interannual and seasonal variability of biomass burning emissions constrained by satellite observations, J.

1038 Geophys. Res., 108, 4040, doi:10.1029/2002JD002378, 2003.
1039
1040 Duncan, B. N., Logan, J. A., Bey, I., Megretskaia, I. A., Yantosca, R. M., Novelli, P. C.,
1041 Jones, N. B., and Rinsland, C. P.: Global budget of CO, 1988-1997: source estimates and
1042 validation with a global model, J. Geophys. Res., 112, D22301,
1043 doi:10.1029/2007JD008459, 2007.
1044
1045 Eckhardt, S., Stohl, A., Wernli, H., James, P., Forster, C., and Spichtinger, N.: A 15-Year
1046 climatology of warm conveyor belts, J. Climate, 17, 218-237, 2004.
1047
1048 Edwards, D. P., Halvorson, C. M., and Gille, J. C.: Radiative transfer modeling for the
1049 EOS Terra satellite measurements of pollution in the troposphere (MOPITT instrument), J.
1050 Geophys. Res., 104, 16755-16775, 1999.
1051
1052 Emmons, L. K., Deeter, M. N., Gille, J. C., Edwards, D. P., Attie, J.-L., Warner, J., Ziskin,
1053 D., Khattatov, B., Yudin, V., Lamarque, J.-F., Ho, S.-P., Mao, D., Chen, J. S., Drummond,
1054 J., Novelli, P., Sachse, G., Coffey, M. T., Hannigan, J. W., Gerbig, C., Kawakami, S.,
1055 Kondo, Y., Takegawa, N., Baehr, J., and Ziereis, H.: Validation of MOPITT CO retrievals
1056 with aircraft in situ profiles, J. Geophys. Res., 109, D03309, doi:10.1029/2003JD004101,
1057 2004.
1058
1059 Giglio, L., Descloitres, J., Justice, C. O., and Kaufman, Y. J.: An enhanced contextual fire
1060 detection algorithm for MODIS, Remote Sens. Environ., 87, 273-282, 2003.
1061
1062 Hao, H., Valks, P., Loyola, D., Chen, Y. F., and Zimmer, W.: Space-based measurements
1063 of air quality during the World Expo 2010 in Shanghai, Environ. Res. Lett., 6, 044004,
1064 doi:10.1088/1748-9326/6/4/044004, 2011.
1065
1066 He, H., Tarasick, D. W., Hocking, W. K., Carey-Smith, T. K., Rochon, Y., Zhang, J.,
1067 Makar, P. A., Osman, M., Brook, J., Moran, M. D., Jones, D. B. A., Mihele, C., Wei, J. C.,
1068 Osterman, G., Argall, P. S., McConnell, J., and Bourqui, M. S.: Transport analysis of
1069 ozone enhancement in Southern Ontario during BAQS-Met, Atmos. Chem. Phys., 11,
1070 2569-2583, doi:10.5194/acp-11-2569-2011, 2011.
1071
1072 Heald, C. L., Jacob, D. J., Fiore, A. M., Emmons, L. K., Gille, J. C., Deeter, M. N.,
1073 Warner, J., Edwards, D. P., Crawford, J. H., Hamlin, A. J., Sachse, G. W., Browell, E. V.,
1074 Avery, M. A., Vay, S. A., Westberg, D. J., Blake, D. R., Singh, H. B., Sandholm, S. T.,
1075 Talbot, R. W., and Fuelberg, H. E.: Asian outflow and transpacific transport of carbon
1076 monoxide and ozone pollution: an integrated satellite, aircraft and model perspective, J.
1077 Geophys. Res., 108, 4804, doi:10.1029/2003JD003507, 2003.
1078
1079 Hocking, W. K., Carey-Smith, T. K., Tarasick, D. W., Argall, P. S., Strong, K., Rochon, Y.,
1080 Zawadzki, I., and Taylor, P. A.: Detection of stratospheric ozone intrusion by wind
1081 profiler radars, Nature, 450, 281-284, doi:10.1038/nature06312, 2007.
1082
1083 Holloway, T., Levy II, H., and Kasibhatla, P.: Global distribution of carbon monoxide, J.

Geophys. Res., 105, 12123-12147, doi:10.1029/1999JD901173, 2000.

Jacob, D. J.: Introduction to Atmospheric Chemistry, Princeton University Press, Princeton, New Jersey, 1999.

Jacob, D. J., Crawford, J. H., Kleb, M. M., Connors, V. S., Bendura, R. J., Raper, J. L., Sachse, G. W., Gille, J. C., Emmons L., and Heald, C. L.: Transport and Chemical Evolution over the Pacific (TRACE-P) aircraft mission: design, execution, and first results, J. Geophys. Res., 108, 9000, doi:10.1029/2002JD003276, 2003.

Jaffe, D., Anderson, T., Covert, D., Kotchenruther, R., Trost, B., Danielson, J., Simpson, W., Berntsen, T., Karlsdottir, S., Blake, D., Harris, J., Carmichael, G., and Uno, I.: Transport of Asian air pollution to North America, Geophys. Res. Lett., 26, 711-714, 1999.

Jaffe, D., Bertschi, I., Jaegle, L., Novelli, P., Reid, J. S., Tanimoto, H., Vingarzan, R.,and Westphal, D. L.: Long-range transport of Siberian biomass burning emissions and impact on surface ozone in western North America, Geophys. Res. Lett., 31, L16106, doi:10.1029/2004GL020093, 2004.

Jiang, Z., Jones, D. B. A., Kopacz, M., Liu, J., Henze, D. K., and Heald, C.: Quantifying the impact of model errors on top-down estimates of carbon monoxide emissions using satellite observations, J. Geophys. Res. 116, D15306, doi:10.1029/2010JD015282, 2011.

Jones, D. B. A., Bowman, K. W., Logan, J. A., Heald, C. L., Liu, J., Luo, M., Worden, J., and Drummond, J.: The zonal structure of tropical O_3 and CO as observed by the Tropospheric Emission Spectrometer in November 2004 - Part 1: Inverse modeling of CO emissions, Atmos. Chem. Phys., 9, 3547-3562, doi:10.5194/acp-9-3547-2009, 2009.

Justice, C. O., Giglio, L., Korontzi, S., Owens, J., Morisette, J. T., Roy, D., Descloitres, J., Alleaume, S., Petitcolin, F., and Kaufman, Y.: The MODIS fire products, Remote Sens. Environ., 83, 244-262, 2002.

Kar, J., Bremer, H., Drummond, J. R., Rochon, Y. J., Jones, D. B. A., Nichitiu, F., Zou, J., Liu, J., Gille, J. C., Edwards, D. P., Deeter, M. N., Francis, G., Ziskin, D., and Warner, J.: Evidence of vertical transport of carbon monoxide from measurements of pollution in the troposphere (MOPITT). Geophys. Res. Lett., 31, L23105, doi:10.1029/2004GL021128, 2004.

Kar, J., Drummond, J. R., Jones, D. B. A., Liu, J., Nichitiu, F., Zou, J., Gille, J. C. Edwards, D. P., Deeter, M. N.: Carbon monoxide (CO) maximum over the Zagros mountains in the Middle East: signature of mountain venting?, Geophys. Res. Lett., 33, L15819, doi:10.1029/2006GL026231, 2006.

Kar, J., Jones, D. B. A., Drummond, J. R., Attie, J. L., Liu, J., Zou, J., Nichitiu, F., Seymour, M. D., Edwards, D. P., Deeter, M. N., Gille, J. C., and Richter, A.:

Measurement of low-altitude CO over the Indian subcontinent by MOPITT, J. Geophys. Res., 113, D16307, doi:10.1029/2007JD009362, 2008.

Kopacz, M., Jacob, D. J., Fisher, J. A., Logan, J. A., Zhang, L., Megretskaia, I. A., Yantosca, R. M., Singh, K., Henze, D. K., Burrows, J. P., Buchwitz, M., Khlystova, I., McMillan, W. W., Gille, J. C., Edwards, D. P., Eldering, A., Thouret, V., and Nédélec, P.: Global estimates of CO sources with high resolution by adjoint inversion of multiple satellite datasets (MOPITT, AIRS, SCIAMACHY, TES), Atmos. Chem. Phys., 10, 855-876, doi:10.5194/acp-10-855-2010, 2010.

Kowol-Santen, J., Beekmann, M., Schmitgen, S., and Dewey, K.: Tracer analysis of transport from the boundary layer to the free atmosphere, Geophys. Res. Lett., 28, 2907-2910, 2001.

Lavoué, D., Liousse, C., Cachier, H., Stocks, B. J., and Goldammer, J. G.: Modeling of carbonaceous particles emitted by boreal and temperate wildfires at northern latitudes, J. Geophys. Res., 105, 26871-26890, doi:10.1029/2000JD900180, 2000.

Lawrence, M. G., Rasch, P. J., von Kuhlmann, R., Williams, J., Fischer, H., de Reus, M., Lelieveld, J., Crutzen, P. J., Schultz, M., Stier, P., Huntrieser, H., Heland, J., Stohl, A., Forster, C., Elbern, H., Jakobs, H., and Dickerson, R. R.: Global chemical weather forecasts for field campaign planning: predictions and observations of large-scale features during MINOS, CONTRACE, and INDOEX, Atmos. Chem. Phys., 3, 267-289, doi:10.5194/acp-3-267-2003, 2003.

Li, Q. B., Jacob, D. J., Park, R. J., Wang, Y. X., Heald, C. L., Hudman, R., Yantosca, R. M., Martin, R. V., and Evans, M. J.: North American pollution outflow and the trapping of convectively lifted pollution by upper-level anticyclone, J. Geophys. Res., 110, D10301, doi:10.1029/2004JD005039, 2005.

Li, Z., Chen, H., Cribb, M., Dickerson, R., Holben, B., Li, C., Lu, D., Luo, Y., Maring, H., Shi, G., Tsay, S.-C., Wang, P., Wang, Y., Xia, X., Zheng, Y., Yuan, T., and Zhao, F.: Preface to special section on East Asian Studies of Tropospheric Aerosols: an International Regional Experiment (EAST-AIRE), J. Geophys. Res., 112, D22S00, doi:10.1029/2007JD008853, 2007.

Liang, Q., Jaegle, L., Jaffe, D. A., Weiss-Penzias, P., Heckman, A., and Snow, J. A.: Long-range transport of Asian pollution to the northeast Pacific: seasonal variations and transport pathways of carbon monoxide, J. Geophys. Res., 109, D23S07, doi:10.1029/2003JD004402, 2004.

Lin, C.-Y., Hsu, H.-m., Lee, Y. H., Kuo, C. H., Sheng, Y.-F., and Chu, D. A.: A new transport mechanism of biomass burning from Indochina as identified by modeling studies, Atmos. Chem. Phys., 9, 7901-7911, doi:10.5194/acp-9-7901-2009, 2009.

Liu, C., Beirle, S., Butler, T., Liu, J., Hoor, P., Jöckel, P., Penning de Vries, M., Pozzer, A.,

Frankenberg, C., Lawrence, M. G., Lelieveld, J., Platt, U., and Wagner, T.: Application of SCIAMACHY and MOPITT CO total column measurements to evaluate model results over biomass burning regions and Eastern China, Atmos. Chem. Phys., 11, 6083-6114, doi:10.5194/acp-11-6083-2011, 2011.

Liu, H. Y., Jacob, D. J., Bey, I., Yantosca, R. M., Duncan, B. N., and Sachse, G.W.: Transport pathways for Asian combustion outflow over the Pacific: interannual and seasonal variations, J. Geophys. Res., 108, 8786, doi:10.1029/2002JD003102, 2003.

Liu, J., Drummond, J. R., Li, Q., Gille, J. C., and Ziskin, D. C.: Satellite mapping of CO emission from forest fires in northwest America using MOPITT measurements, Remote Sens. Environ., 95, 502-516, 2005.

Liu, J., Drummond, J. R., Jones, D. B. A., Cao, Z., Bremer, H., Kar, J., Zou, J., Nichitiu, F., and Gille, J. C.: Large horizontal gradients in atmospheric CO at the synoptic scale as seen by spaceborne measurements of pollution in the troposphere, J. Geophys. Res., 111, D02306, doi:10.1029/2005JD006076, 2006.

Mari, C., Evans, M. J., Palmer, P. I., Jacob, D. J., and Sachse, G. W.: Export of Asian pollution during two cold front episodes of the TRACE-P experiment, J. Geophys. Res., 109, D15S17, doi:10.1029/2003JD004307, 2004.

Miyazaki, Y., Kondo, Y., Koike, M., Fuelberg, H. E., Kiley, C. M., Kita, K., Takegawa, N., Sachse, G. W., Flocke, F., Weinheimer, A. J., Singh, H. B., Eisele, F. L., Zondlo, M., Talbot, R. W., Sandholm, S. T., Avery, M. A., and Blake, D. R.: Synoptic-scale transport of reactive nitrogen over the western Pacific in spring, J. Geophys. Res., 108, 8788, doi:10.1029/2002JD003248,2003.

Marenco, A., Thouret, V., Nédélec, P., Smit, H., Helten, M., Kley, D., Karcher, F., Simon, P., Law, K., Pyle, J., Poschmann, G., Wrede, R. V., Hume, C., and Cook, T: Measurement of ozone and water vapor by Airbus in-service aircraft: the MOZAIC airborne program, An overview, J. Geophys. Res., 103, 25631-25642, 1998.

Nassar, R., Logan, J. A., Megretskaia, I. A., Murray, L. T., Zhang, L., and Jones, D. B. A.: Analysis of tropical tropospheric ozone, carbon monoxide, and water vapor during the 2006 El Niño using TES observations and the GEOS-Chem model, J. Geophys. Res., 114, D17304, doi:10.1029/2009JD011760, 2009.

Nassar, R., Jones, D. B. A., Suntharalingam, P., Chen, J. M., Andres, R. J., Wecht, K. J., Yantosca, R. M., Kulawik, S. S., Bowman, K. W., Worden, J. R., Machida, T., and Matsueda, H.: Modeling global atmospheric CO_2 with improved emission inventories and CO_2 production from the oxidation of other carbon species, Geosci. Model Dev., 3, 689-716, doi:10.5194/gmd-3-689-2010, 2010.

Nédélec, P., Thpuret, V., Brioude, J., Sauvage, B., Cammas, J., Stohl, A.: Extreme CO concentrations in the upper troposphere over northeast Asia in June 2003 from the in situ

MOZAIC aircraft data, Geophys. Res. Lett., 32, L14807, doi:10.1029/2005GL023141, 2005.

Novelli, P., Masarie, K. A., and Lang, P. M.: Distributions and recent changes of carbon monoxide in the lower troposphere, J. Geophys. Res., 103, 19015 - 19033, 1998.

Olivier, J. G. J. and Berdowski, J. J. M.: Global emission sources and sinks, in: The Climate System, edited by: Berdowski, J., Guicherit, R., and Heij, B. J., Swets & Zeitlinger, Lisse, the Netherlands, 33 -77, 2001.

Oltmans, S. J., Lefohn, A. S., Harris, J. M., Tarasick, D. W., Thompson, A. M., Wernli, H., Johnson, B. J., Novelli, P. C., Montzka, S. A., Ray, J. D., Patrick, L. C., Sweeney, C., Jefferson, A., Dann, T., Davies, J., Shapiro, M., Holben, B. N.: Enhanced ozone over western North America from biomass burning in Eurasia during April 2008 as seen in surface and profile observations, Atmos. Environ., 44, 4497-4509, 2010.

Pan, L., Gille, J. C., Edwards, D. P., Bailey, P. L., and Rodgers, C. D.: Retrieval of tropospheric carbon monoxide for the MOPITT experiment, J. Geophys. Res., 103, 32277-32290, 1998.

Pickering, K. E., Dickerson, R. R., Huffman, G. J., Boatman, J. F., and Schanot, A.: Trace gas transport in the vicinity of frontal convective clouds, J. Geophys. Res., 93, 759 -773, doi:10.1029/JD093iD01p00759, 1998.

Randel, W. J., Park, M., Emmons, L., Kinnison, D., Bernath, P., Walker, K. A., Boone, C., and Pumphrey, H.: Asian monsoon transport of pollution to the stratosphere, Science, 328, 611-613, doi:10.1126/science.1182274, 2010.

Rogers, C. D.: Inverse Methods for Atmospheric Sounding, Theory and Practice, World Sci., River Edge, N.J., 2000.

Schultz, M. G.: On the use of ATSR fire count data to estimate the seasonal and interannual variability of vegetation fire emissions, Atmos. Chem. Phys., 2, 387-395, doi:10.5194/acp-2-387-2002, 2002.

Stohl, A.: A 1-year Lagrangian ``climatology" of airstreams in the North Hemisphere troposphere and lowermost stratosphere,~J. Geophys. Res., 106,7263-7279, 2001.

Stohl, A., Hittenberger, M., and Wotawa, G.: Validation of the Lagrangian particle dispersion model FLEXPART against large scale tracer experiment data, Atmos. Environ., 24, 4245-4264, 1998.

Stohl, A., Eckhardt, S., Forster, C., James, P., and Spichtinger, N.: On the pathways and timescales of intercontinental air pollution transport, J. Geophys. Res., 107, 4684, doi:10.1029/2001JD001396, 2002.

Stohl, A., Forster, C., Frank, A., Seibert, P., and Wotawa, G.: Technical note: The Lagrangian particle dispersion model FLEXPART version 6.2, Atmos. Chem. Phys., 5, 2461-2474, doi:10.5194/acp-5-2461-2005, 2005.

Streets, D. G., Zhang, Q., Wang, L., He, K., Hao, J., Wu, Y., Tang, Y., and Carmichael, G. R.: Revisiting China's CO emissions after the Transport and Chemical Evolution over the Pacific (TRACE-P) mission: synthesis of inventories, atmospheric modeling, and observations, J. Geophys. Res., 111, D14306, doi:10.1029/2006JD007118, 2006.

Su, M., Lin, Y., Fan, X., Peng, L., Zhao, C.: Impacts of global emissions of CO, NO_x, and CH_4 on China tropospheric hydroxyl free radicals, Adv. Atmos. Sci., 29, 4, 838-854, 2012.

Suntharalingam, P., Jacob, D. J., Palmer, P. I., Logan, J. A., Yantosca, R. M., Xiao, Y., Evans, M. J., Streets, D., Vay, S. A., and Sachse, G.: Improved quantification of Chinese carbon fluxes using CO_2/CO correlations in Asian outflow, J. Geophys. Res., 109, D18S18, doi:10.1029/2003JD004362, 2004.

Tao, S. and Ding, Y.: Observational evidence of the influence of the Qinghai-Xizang (Tibet) Plateau on the occurrence of heavy rain and severe convective storms in China, B. Am. Meteorol. Soc., 62, 2-30, 1981.

Tanimoto, H., Sawa, Y., Yonemura, S., Yumimoto, K., Matsueda, H., Uno, I., Hayasaka, T., Mukai, H., Tohjima, Y., Tsuboi, K., and Zhang, L.: Diagnosing recent CO emissions and ozone evolution in East Asia using coordinated surface observations, adjoint inverse modeling, and MOPITT satellite data, Atmos. Chem. Phys., 8, 3867-3880, doi:10.5194/acp-8-3867-2008, 2008.

Tsutsumi, Y., Makino, Y., and Jensen, J. B.: Vertical and latitudinal distributions of tropospheric ozone over the western Pacific: case studies from the PACE aircraft missions, J. Geophys. Res., 108, 4251, doi:10.1029/2001JD001374, 2003.

van der Werf, G. R., Randerson, J. T., Giglio, L., Collatz, G. J., Mu, M., Kasibhatla, P. S., Morton, D. C., DeFries, R. S., Jin, Y., and van Leeuwen, T. T.: Global fire emissions and the contribution of deforestation, savanna, forest, agricultural, and peat fires (1997-2009), Atmos. Chem. Phys., 10, 11707--11735, doi:10.5194/acp-10-11707-2010, 2010.

Wang, T., Nie, W., Gao, J., Xue, L. K., Gao, X. M., Wang, X. F., Qiu, J., Poon, C. N., Meinardi, S., Blake, D., Wang, S. L., Ding, A. J., Chai, F. H., Zhang, Q. Z., and Wang, W. X.: Air quality during the 2008 Beijing Olympics: secondary pollutants and regional impact, Atmos. Chem. Phys., 10, 7603-7615, doi:10.5194/acp-10-7603-2010, 2010.

Wang, X. L., Feng, Y., Compo, G. P., Swail, V. R., Zwiers, F. W., Allan, R. J., and Sardeshmukh, P. D.: Trends and low frequency variability of extra-tropical cyclone activity in the ensemble of twentieth century reanalysis, Clim. Dynam., 40, 2775-2800, doi:10.1007/s00382-012-1450-9, 2013.

Wofsy, S. C., and the HIPPO Science Team and Cooperating Modellers and Satellite Teams: HIAPER pole-to-pole observations (HIPPO): Fine-grained, global-scale measurements of climatically important atmospheric gases and aerosols, Phil. Trans. R. Soc. A, 369, 2073–2086, doi:10.1098/rsta.2010.0313, 2011.

Worden, H. M., Deeter, M. N., Edwards, D. P., Gille, J. C., Drummond, J. R., and Nédélec, P.: Observations of near-surface carbon monoxide from space using MOPITT multispectral retrievals, J. Geophys. Res., 115, D18314, doi:10.1029/2010JD014242, 2010.

Wotawa, G., Novelli, P. C., Trainer, M., and Granier, C.: Interannual variability of summertime CO concentrations in the Northern Hemisphere explained by boreal forest fires in North America and Russia, Geophys. Res. Lett., 28, 4575-4578, 2001.

Yienger, J. J., Galanter, M., Holloway, T. A., Phadnis, M. J., Guttikunda, S. K., Carmichael, G. R., Moxim, W. J., and Levy II, H.: The episodic nature of air pollution transport from Asia to North America, J. Geophys. Res., 105, 26931-26945, doi:10.1029/2000JD900309, 2000.

Yu, R., Xu, Y., Zhou, T., and Li, J.: Relation between rainfall duration and diurnal variation in the warm season precipitation over central eastern China, Geophys. Res. Lett., 34, Li3703, doi:10.1029/2007GL030315, 2007.

Yue, X. and Wang, H.: The springtime North Asia cyclone activity index and the Southern Annular Mode, Adv. Atmos. Sci., 25, 673-679, 2008.

Yurganov, L. N., McMillan, W. W., Dzhola, A. V., Grechko, E. I., Jones, N. B., and van derWerf, G.: Global AIRS and MOPITT CO measurements: validation, comparison, and links to biomass burning variations and carbon cycle, J. Geophys. Res., 113, D09301, doi:10.1029/2007JD009229, 2008.

Zhang, L., Jacob, D. J., Bowman, K. W., Logan, J. A., Turquety, S., Hudman, R. C., Li, Q. B., Beer, R., Worden, H. M., Worden, J. R., Rinsland, C. P., Kulawik, S. S., Lampel, M. C., Shephard, M. W., Fisher, B. M., Eldering, A., and Avery, M. A.: Ozone-CO correlations determined by the TES satellite instrument in continental outflow regions, Geophys. Res. Lett., 33, L18804, doi:10.1029/2006GL026399, 2006.

Zhang, Q., Streets, D. G., Carmichael, G. R., He, K. B., Huo, H., Kannari, A., Klimont, Z., Park, I. S., Reddy, S., Fu, J. S., Chen, D., Duan, L., Lei, Y., Wang, L. T., and Yao, Z. L.: Asian emissions in 2006 for the NASA INTEX-B mission, Atmos. Chem. Phys., 9, 5131-5153, doi:10.5194/acp-9-5131-2009, 2009.

Zhao, C., Wang, W., Yang, Y., Fu, R., Cunnold, D., and Choi, Y.: Impact of East Asian summer monsoon on the air quality over China: view from space, J. Geophys. Res., 115, D09301, doi:10.1029/2009JD012745, 2010.

Zhao, T. L., Gong, S. L., Zhang, X. Y., and Jaffe, D. A.: Asian dust storm influence on North American ambient PM levels: observational evidence and controlling factors, Atmos. Chem. Phys., 8, 2717-2728, doi:10.5194/acp-8-2717-2008, 2008.

Zhou, D., Ding, A., Mao, H., Fu, C., Wang, T., Chan, L. Y., Ding, K., Zhang, Y., Liu, J., Lu, A., and Hao, N.: Impacts of the East Asian monsoon on lower tropospheric ozone over coastal South China, Environ. Res. Lett., 8, 044011, doi:10.1088/1748-9326/8/4/044011, 2013.

Figure caption

Fig. 1. The Degree of Freedom for Signal (DFS) of the MOPITT V5 TIR/NIR data over East Asia, averaged for 2005 during (a) daytime and (b) nighttime. Locations of four cities with MOZAIC CO measurements are indicated as stars. Note that the MOZAIC CO data from Narita also include a small portion of measurements from its surrounding cities at Osaka and Nagoya.

Fig. 2. Relative bias of CO profiles (in %) between MOPITT and MOZAIC data (smoothed with the MOPITT averaging kernels, see Equation 1) from 2003 to 2005 at Beijing, Narita, Shanghai, and Hong Kong for MOPITT V4 and V5 data. The number of profiles for the comparison is 18, 23, 11, and 15, respectively, at Beijing, Narita, Shanghai, and Hong Kong. The error bars indicate the interquartile range of the mean.

Fig. 3. Correlation between MOPITT and MOZAIC data (smoothed with the MOPITT averaging kernels, see Equation 1) from 2003 to 2005 at Beijing, Narita, Shanghai, and Hong Kong (a) from the middle to upper troposphere and (b) from the surface to the middle troposphere.

Fig. 4. MOPITT CO mixing ratio (ppbv, in color) (a) on 6 June 2003 at 500 hPa, (b) on 18 March 2004 at 700 hPa, and (c) on April 10, 2005 at 300 hPa. All are overlaid with horizontal winds (in arrows) at the same altitude. In each subfigure, the locations of MOZAIC data at 900, 600, and 300 hPa are indicated as red, blue and pink dots, respectively. The box indicates an area over which mean MOPITT CO profile are taken and displayed in Fig.5. The box is selected to ensure enough MOPITT samplings at the closest upwind direction of MOZAIC measurements. The two blue dashed lines define the longitudinal zone, over which the CO abundances were averaged and shown in Fig 6. The solid blue bars in Figs. 4a and 4c indicate the locations where particles were released and backward trajectories were simulated using FLEXPART (see text for detail).

Fig. 5. Profiles of MOPITT CO and the a priori, averaged over the corresponding boxed area in Fig. 4 on (a) 6 June 2003, (c) 18 March 2004, and (e) 10 April 2005, respectively, along with their monthly mean MOPITT CO profile over the same area. The corresponding MOZAIC CO profiles (along the dots in Fig. 4) on the same day are shown in (b), (d), and (f), respectively. The corresponding MOZAIC ozone and relative humidity profiles are also shown in (b), (d), and (f). Note that the smoothed MOZAIC

CO profiles (MOZAIC CO(s)) were calculated using the averaging kernels and the a priori in the boxed area in each case (see Sect. 5 for discussion).

Fig. 6. A latitude-altitude cross section of MOPITT CO averaged between the two blue dashed lines in Fig.4 on (a) June 6, 2003, (b) March 18, 2004, and (c) April 10, 2005. The contour lines indicate U wind speed (m s^{-1}). Vectors are for wind directions in V and W. For a better illustration, W is enlarged by a factor of 100. The pink box(es) in (a) and (c) indicate the locations where particles were released and backward trajectories were simulated using FLEXPART (see text for detail).

Fig. 7. (a) Particle distribution between 6.25-10.25 km (~550-250 hPa) during June 1-6, 2003. The particles were released from two locations (in pink lines) around 400 hPa (also see Figs. 4a and 6a) on June 6, 2003 and backward trajectories were calculated. The contour lines are the geopotential heights at 850 hPa on June 3, 2003. A cold front and a warm front are indicated by green and red lines, respectively. (b) The same as (a), but between 0-3.5 km. The contour lines are the geopotential heights at 850 hPa on 2 June 2003. The circles, diamonds, and stars denote daily mean fire counts of 20-100, 100-300, and 300-500 per 2.5×2.5 °grid area, respectively, from May 31 to June 6.

Fig. 8. Vertical distribution of particles, varying with time from 1 June 2003 at 0 UTC to 16 June 2003 at 0 UTC. The particles were released from fire regions in Fig. 7b from the surface to 3 km on 1 June 2003 and forward trajectories were calculated (15 days). The forward time (in hour) and date (in June) are indicated in the x-axis on the bottom and the top, respectively.

Fig. 9. MOPITT CO mixing ratio at 700 hPa from 11-19 March 2004, overlaid with the geopotential height at 850 hPa on 17 March 2004 in blue contour and with a front shown by brown solid line. The large and small stars denote daily mean fire counts of 100-200 and over 200 per 2.5×2.5 °grid area during the period, respectively. “L” and “H” indicate a low and high pressure system, respectively.

Fig. 10. (a) CO, (b) CO from biomass burning, and (c) CO from the anthropogenic source on March 18, 2004 at 0 UTC, simulated by GEOS-Chem. The geopotential height at 700 hPa is indicated with white lines. “L” indicates a low pressure system.

Fig. 11. Latitude-altitude cross sections along 130°E of (a) CO, (b) CO from biomass burning, and (c) anthropogenic CO on March 17, 2004 at 6 UTC, simulated by GEOS-Chem. The contour lines indicate U wind speed (m s^{-1}). Vectors are for wind directions in V and W. For a better illustration, W is enlarged by a factor of 100.

Fig. 12. A longitude-altitude cross section of CO along 22°N on March 17, 2004 at 6 UTC, simulated by GEOS-Chem. The topography of the Hengduan Mountains is indicated in white.

Fig. 13. MOPITT CO mixing ratio at 800 hPa from April 3-10, 2005, overlaid with the geopotential height at 850 hPa on April 9, 2005 at 0 UTC in blue contour and with a front

in brown solid line. The large and small stars denote daily mean fire counts of 100-200 and over 200 per 2.5×2.5 °grid area during the period, respectively. The boxed area was identified as a major CO source region from the FLEXPART simulation (see text for detail).

Fig. 14. The GEOS-Chem simulated CO (a) on April 8, 2005 in the lower troposphere (800-700 hPa), (b) on April 9 in the middle troposphere (500-400 hPa), and (c) on April 10 in the upper troposphere (300-200 hPa). The contours are the geopotential height at 850, 450, and 250 hPa, respectively.

Fig. 15. The GEOS-Chem simulated fractional CO (a) from biomass burning and (b) from the anthropogenic source on April 10, 2005 at 00 UTC in the middle troposphere (500-400 hPa). (c) and (d) are the same as for (a) and (b), respectively, but in the upper troposphere (300-200 hPa). The geopotential height at 450 and 250 hPa is overlaid with the CO images in the middle and upper troposphere, respectively. White dots indicate the location of MOZAIC measurements.

Table caption

Table 1. Characterization of the three cases.

Table 2. Occurrences of various CO ranges at different altitudes in the MOZAIC measurements in the vicinity of Narita from 2001 to 2006.

Table 3. Occurrences of various CO ranges at different altitudes in GEOS-Chem simulations and MOPITT observations in the vicinity of Narita (126-140 °E 30-40 °N) in 2005.

Table 1. Characterization of the three cases.

Case	2003	2004	2005
Date	6 June 2003	18 March 2004	10 April 2005
Maximum CO (ppbv) in MOZAIC profiles	~550	~500	~300
CO peak height (hPa) in MOZAIC profiles	500-350	750-550	350-250
Maximum CO (ppbv) in MOPITT images	300-400	200-250	150-200
CO peak height (hPa) in MOPITT images	650-300	750-500	400-250
Peak CO area in MOPITT images	35-55°N 125-145°E	20-32°N 125-135°E	32-37°N 130-140°E
Major CO sources	Large fires near Lake Baikal in Russia	Fires in the Indochina peninsula, anthropogenic emissions in the North China Plain	Fires in the Indochina peninsula, anthropogenic emissions in the North China Plain and the Sichuan basin
Vertical transport mechanism	Frontal lifting	Convection, frontal lifting, and orographic lifting	Convection, frontal lifting, and orographic lifting
Outflow	West coast of Canada	West coast of the United States	West coast of Canada

Table 2. Occurrences of various CO ranges at different altitudes in the MOZAIC measurements in the vicinity of Narita from 2001 to 2006.

Season	Pressure	Occurrence						Fractional Occurrence (%)					
		CO Concentration Range (ppbv)						CO Concentration Range (ppbv)					
	(hPa)	0-100	100-200	200-300	300-400	>400	All	0-100	100-200	200-300	300-400	>400	All
All	400-200	67	354	93	19	6	539	12	66	17	4	1	100
	600-400	36	359	69	15	8	487	7	74	14	3	2	100
	850-600	17	180	150	31	6	384	4	47	39	8	2	100
	Surface-850	4	60	142	83	88	377	1	16	38	22	23	100
Spring	400-200	11	96	28	12	2	149	7	64	19	8	1	100
	600-400	1	101	29	9	3	143	1	71	20	6	2	100
	850-600	0	38	55	20	5	118	0	32	47	17	4	100
	Surface-850	0	14	44	27	29	114	0	12	39	24	25	100
Summer	400-200	14	132	41	4	4	195	7	68	21	2	2	100
	600-400	13	138	22	1	2	176	7	78	13	1	1	100
	850-600	14	80	50	6	0	150	9	53	33	4	0	100
	Surface-850	4	32	48	30	36	150	3	21	32	20	24	100
Fall	400-200	30	61	15	2	0	108	28	56	14	2	0	100
	600-400	20	50	11	2	1	84	24	60	13	2	1	100
	850-600	3	30	17	3	0	53	6	57	32	6	0	100
	Surface-850	0	10	20	12	11	53	0	19	38	23	21	100
Winter	400-200	12	65	9	1	0	87	14	75	10	1	0	100
	600-400	2	70	7	3	2	84	2	83	8	4	2	100
	850-600	0	32	28	2	1	63	0	51	44	3	2	100
	Surface-850	0	4	30	14	12	60	0	7	50	23	20	100

Table 3. Occurrences of various CO ranges at different altitudes in GEOS-Chem simulations and MOPITT observations in the vicinity of Narita (126-140 °E 30-40 °N) in 2005.

Pressure (hPa)	GEOS-Chem: Fractional Occurrence (%) CO Range (ppbv) 0-100	100-200	200-300	300-400	>400	All
200-100	12	87	1	0	0	100
400-200	0	87	12	1	0	100
600-400	0	53	35	11	1	100
850-600	0	20	46	25	8	100
1000-850	0	7	46	35	11	100

Pressure (hPa)	MOPITT: Fractional Occurrence (%) CO Range (ppbv) 0-100	100-200	200-250	>250	All
200-100	38	45	11	6	100
400-200	4	68	18	10	100
600-400	6	86	6	1	100
800-600	7	67	20	6	100
1000-800	2	16	18	64	100

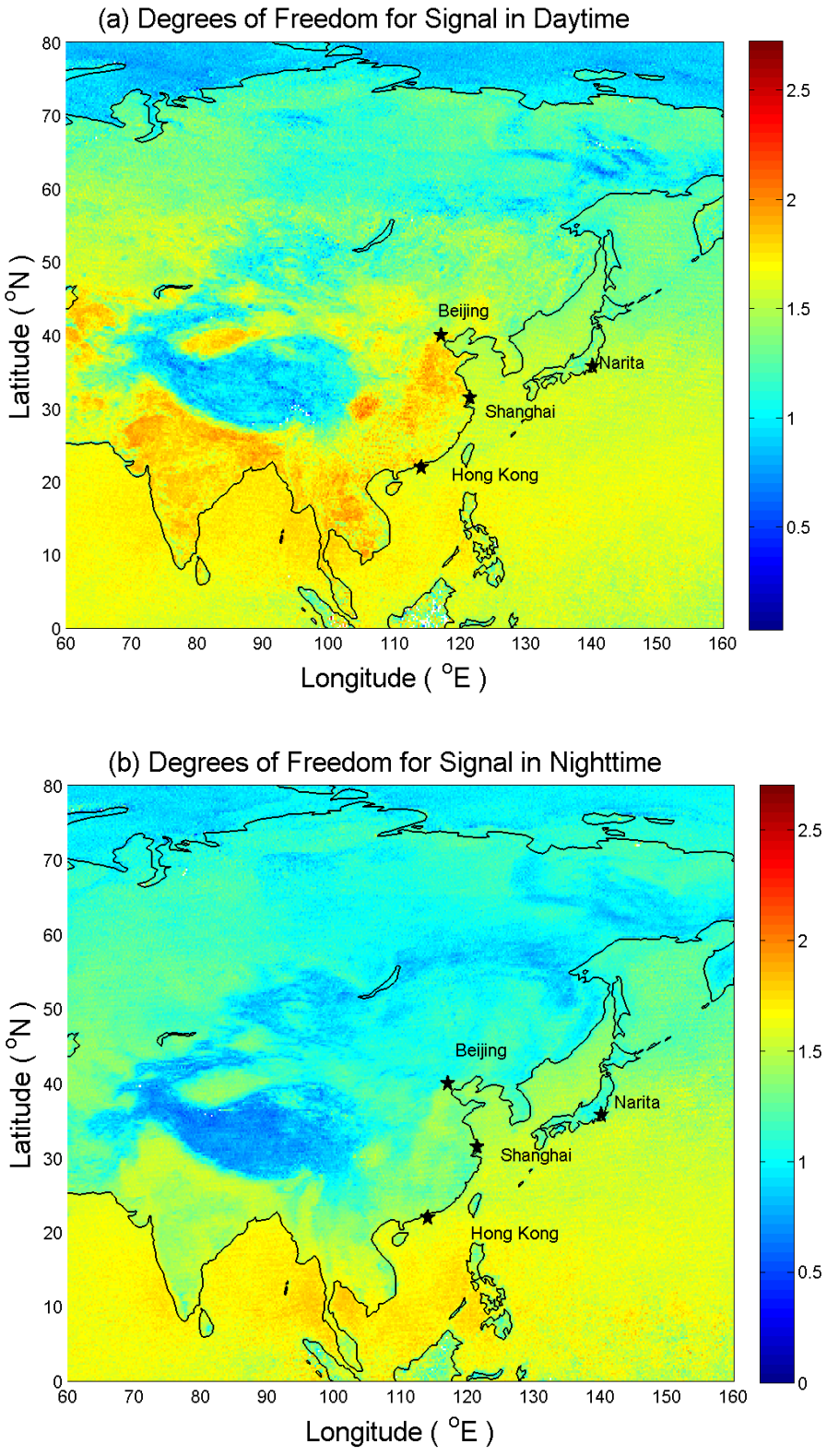

Fig. 1. The Degree of Freedom for Signal (DFS) of the MOPITT V5 TIR/NIR data over East Asia, averaged for 2005 during (a) daytime and (b) nighttime. Locations of four cities with MOZAIC CO measurements are indicated as stars. Note that the MOZAIC CO data from Narita also include a small portion of measurements from its surrounding cities at Osaka and Nagoya.

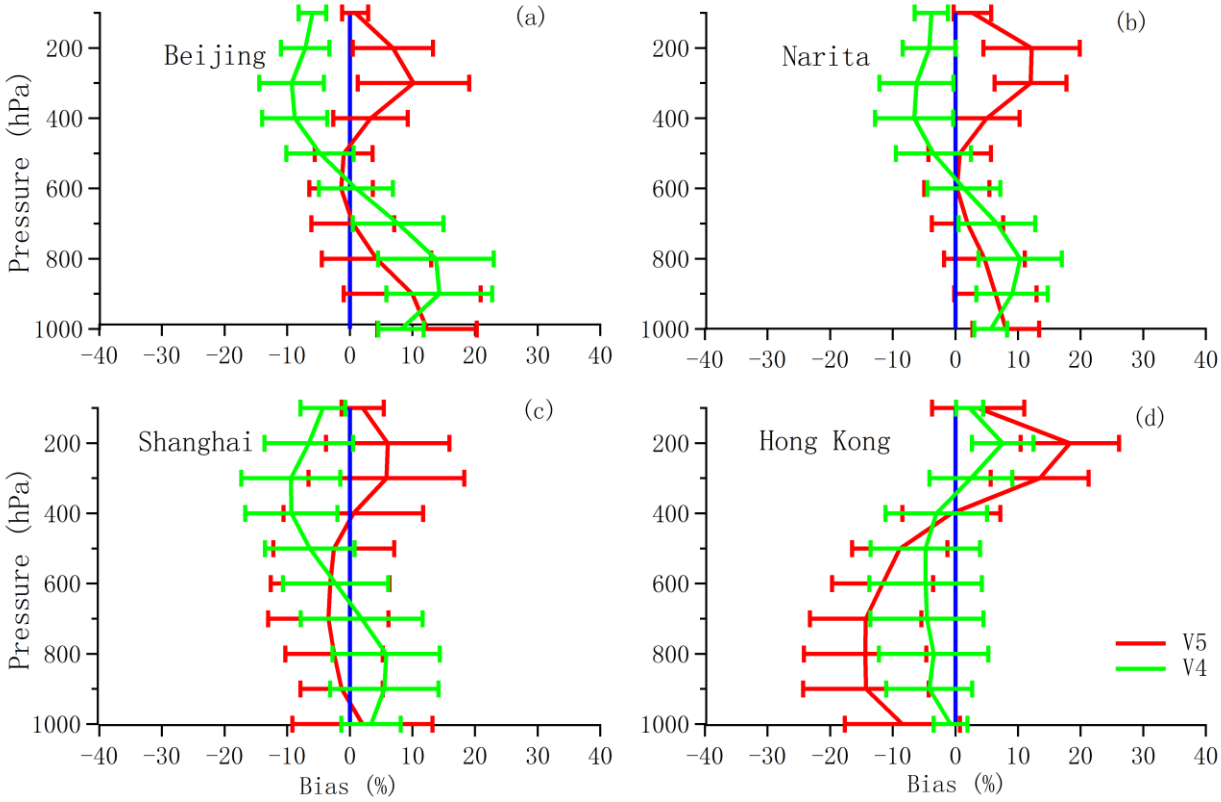

Fig. 2. Relative bias of CO profiles between MOPITT and MOZAIC data (smoothed with the MOPITT averaging kernels, see Equation 1) from 2003 to 2005 at Beijing, Narita, Shanghai, and Hong Kong for MOPITT V4 and V5 data. The number of profiles for the comparison is 18, 23, 11, and 15, respectively, at Beijing, Narita, Shanghai, and Hong Kong. The error bars indicate the interquartile range of the mean.

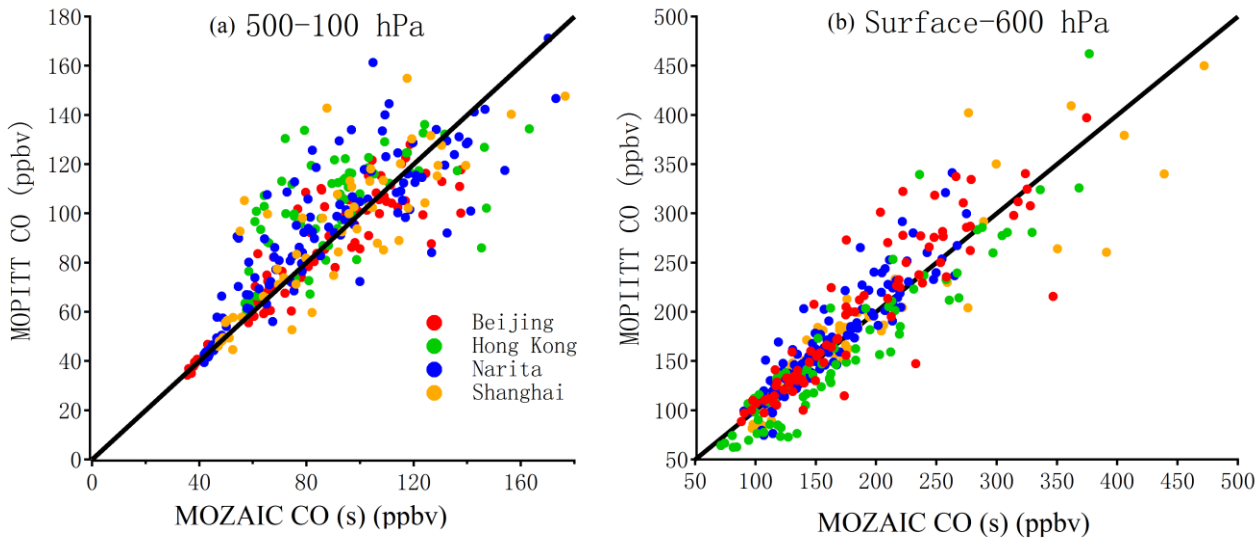

Fig. 3. Correlation between MOPITT and MOZAIC data (smoothed with the MOPITT averaging kernels, see Equation 1) from 2003 to 2005 at Beijing, Narita, Shanghai, and Hong Kong (a) from the middle to upper troposphere and (b) from the surface to the middle troposphere.

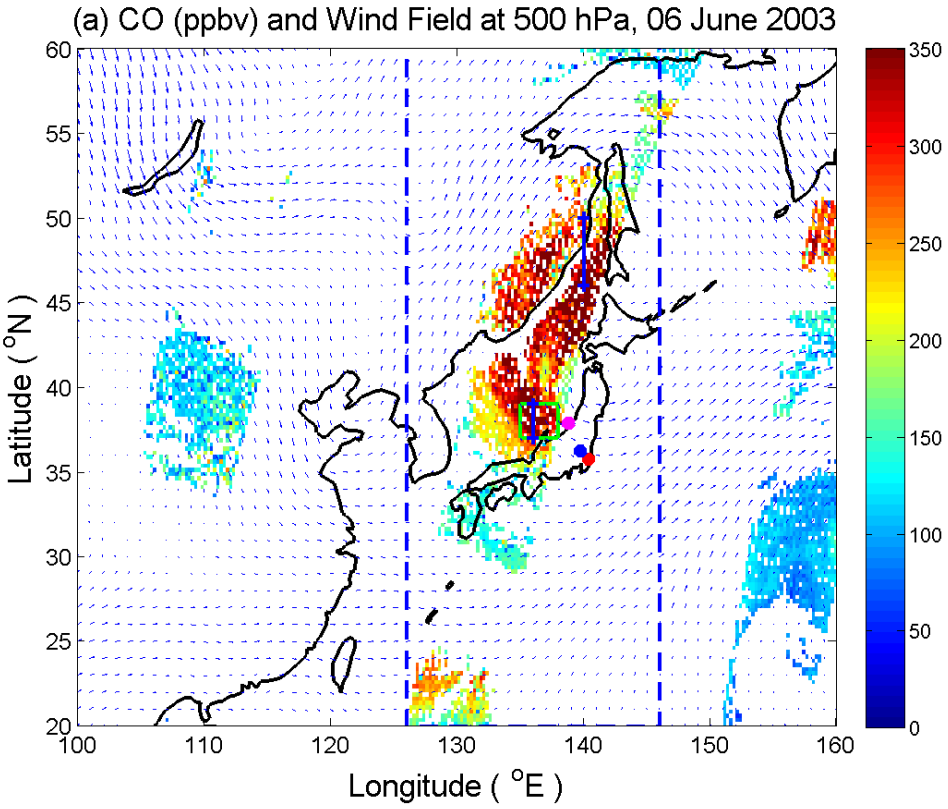
(a) CO (ppbv) and Wind Field at 500 hPa, 06 June 2003
Latitude (°N)
Longitude (°E)
60
55
50
45
40
35
30
25
20
100
110
120
130
140
150
160
350
300
250
200
150
100
50
0

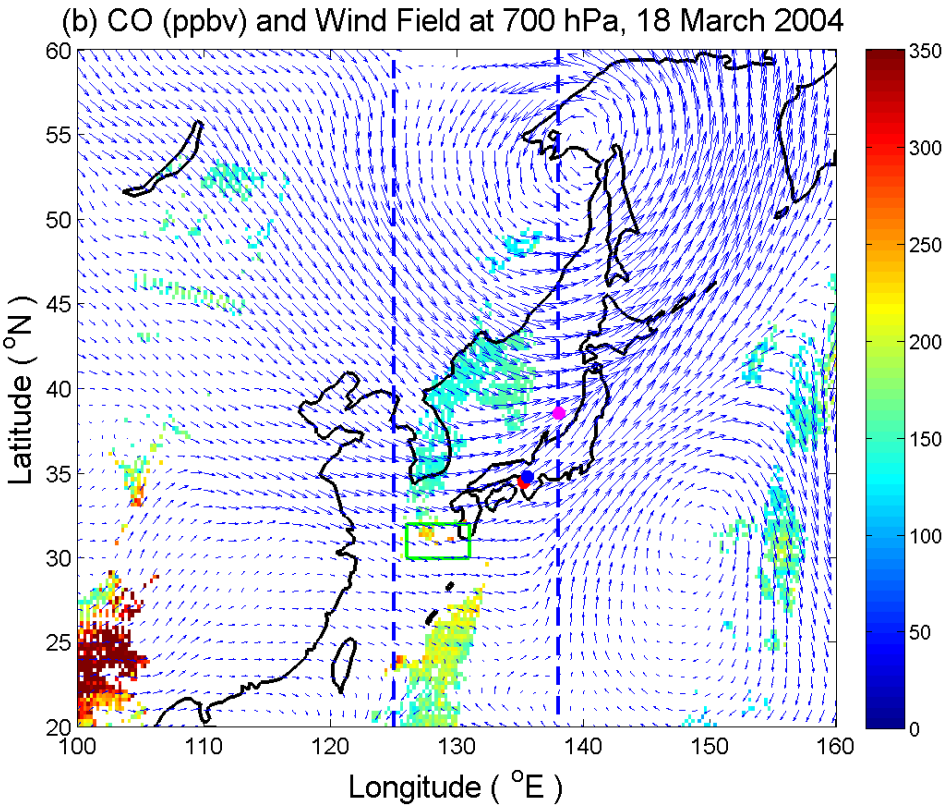
(b) CO (ppbv) and Wind Field at 700 hPa, 18 March 2004
Latitude (°N)
Longitude (°E)
60
55
50
45
40
35
30
25
20
100
110
120
130
140
150
160
350
300
250
200
150
100
50
0

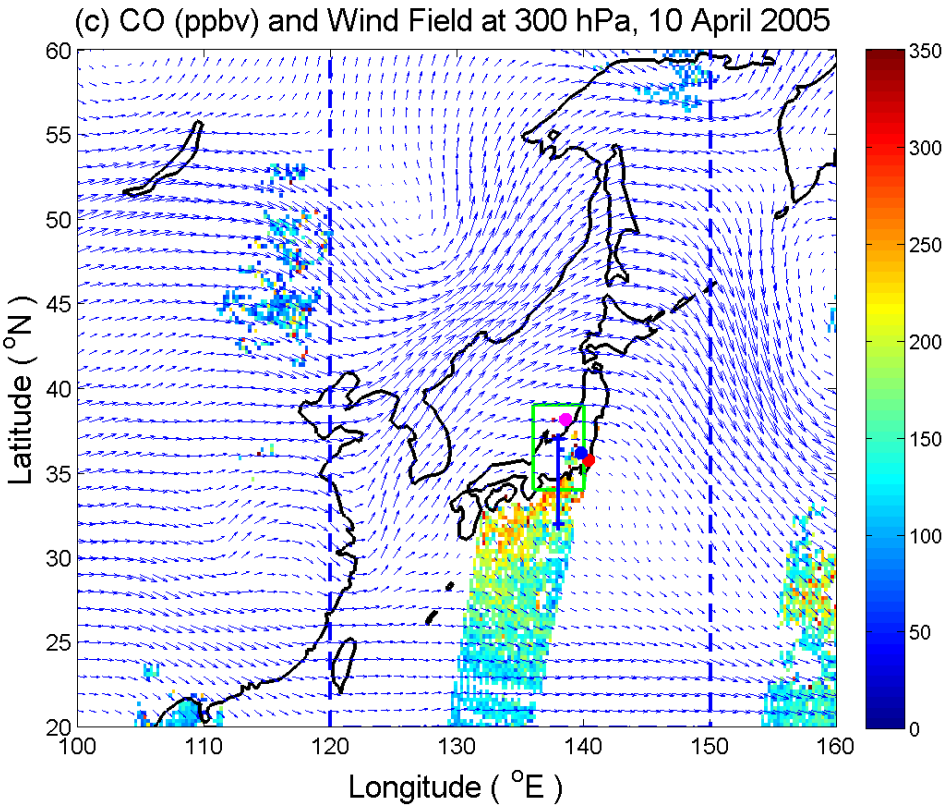

Fig. 4. MOPITT CO mixing ratio (ppbv, in color) (a) on 6 June 2003 at 500 hPa, (b) on 18 March 2004 at 700 hPa, and (c) on April 10, 2005 at 300 hPa. All are overlaid with horizontal winds (in arrows) at the same altitude. In each subfigure, the locations of MOZAIC data at 900, 600, and 300 hPa are indicated as red, blue and pink dots, respectively. The box indicates an area over which mean MOPITT CO profile are taken and displayed in Fig.5. The box is selected to ensure enough MOPITT samplings at the closest upwind direction of MOZAIC measurements. The two blue dashed lines define the longitudinal zone, over which the CO abundances were averaged and shown in Fig 6. The solid blue bars in Figs. 4a and 4c indicate the locations where particles were released and backward trajectories were simulated using FLEXPART (see text for detail).

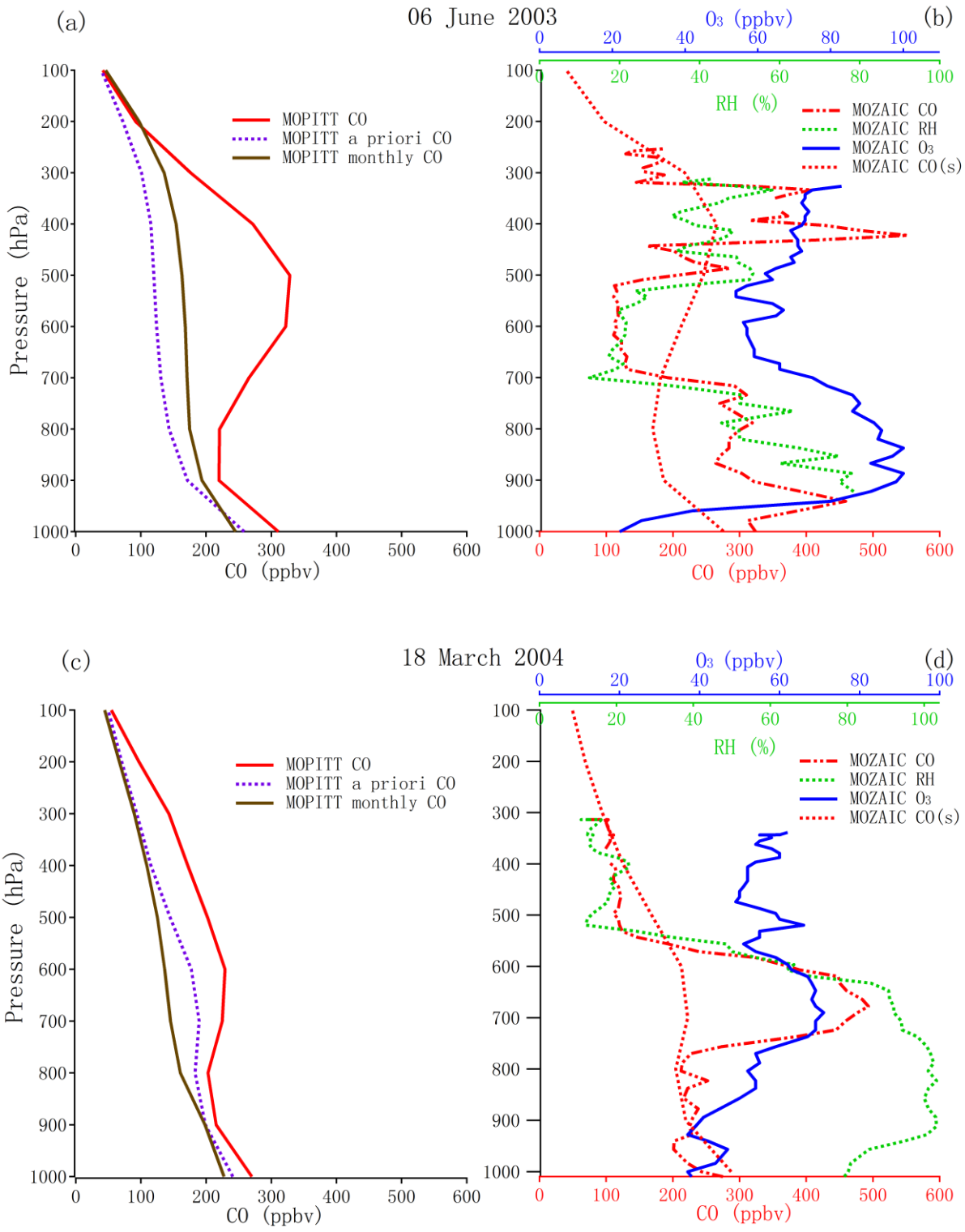
(a)
06 June 2003
(b)
(c)
18 March 2004
(d)
Pressure (hPa)
CO (ppbv)
MOPITT CO
MOPITT a priori CO
MOPITT monthly CO
O3 (ppbv)
RH (%)
MOZAIC CO
MOZAIC RH
MOZAIC O3
MOZAIC CO(s)

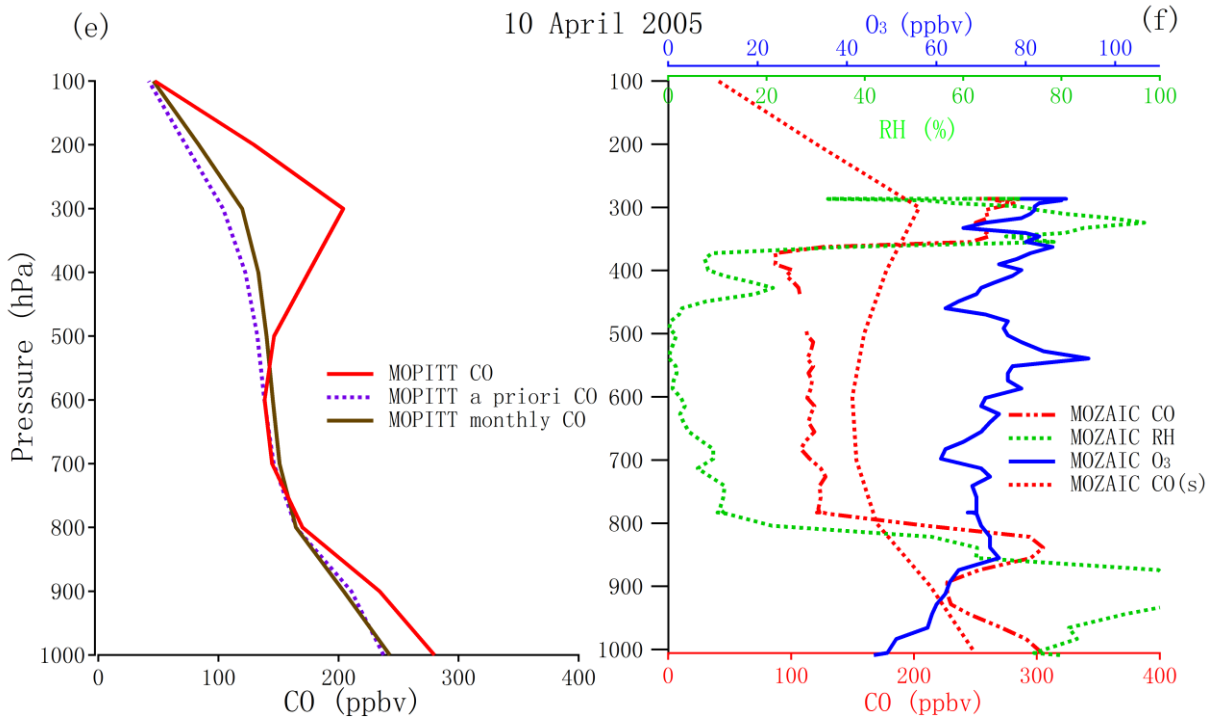

Fig. 5. Profiles of MOPITT CO and the a priori, averaged over the corresponding boxed area in Fig. 4 on (a) 6 June 2003, (c) 18 March 2004, and (e) 10 April 2005, respectively, along with their monthly mean MOPITT CO profile over the same area. The corresponding MOZAIC CO profiles (along the dots in Fig. 4) on the same day are shown in (b), (d), and (f), respectively. The corresponding MOZAIC ozone and relative humidity profiles are also shown in (b), (d), and (f). Note that the smoothed MOZAIC CO profiles (MOZAIC CO(s)) were calculated using the averaging kernels and the a priori in the boxed area in each case (see Sect. 5 for discussion).

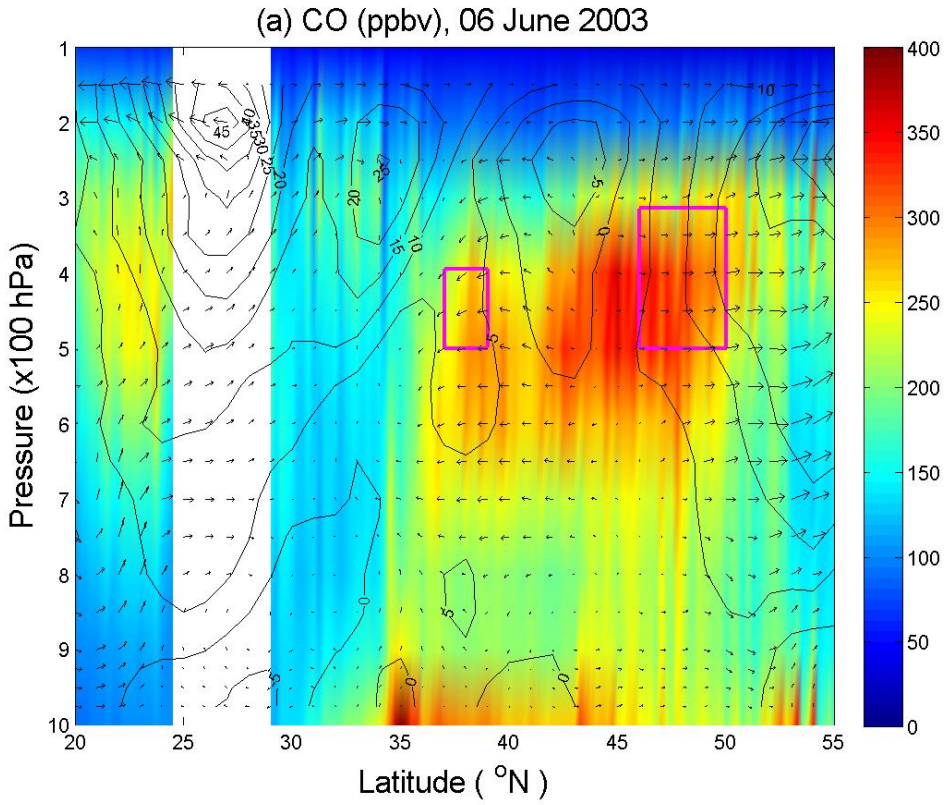
(a) CO (ppbv), 06 June 2003
Pressure (x100 hPa)
Latitude (°N)

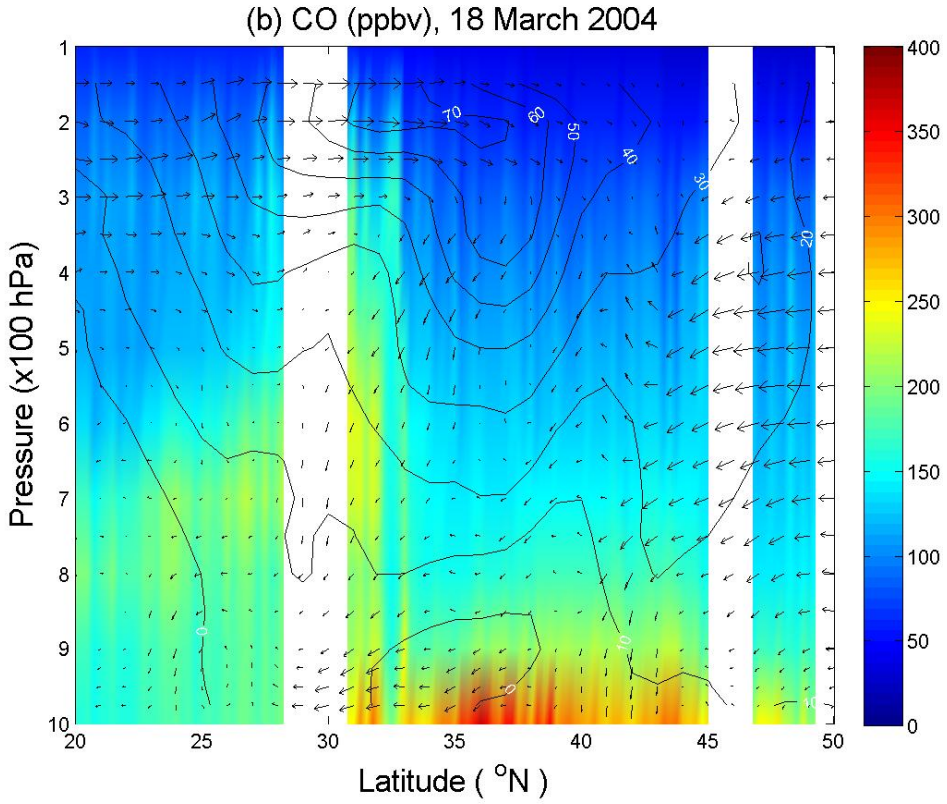
(b) CO (ppbv), 18 March 2004
Pressure (x100 hPa)
Latitude (°N)

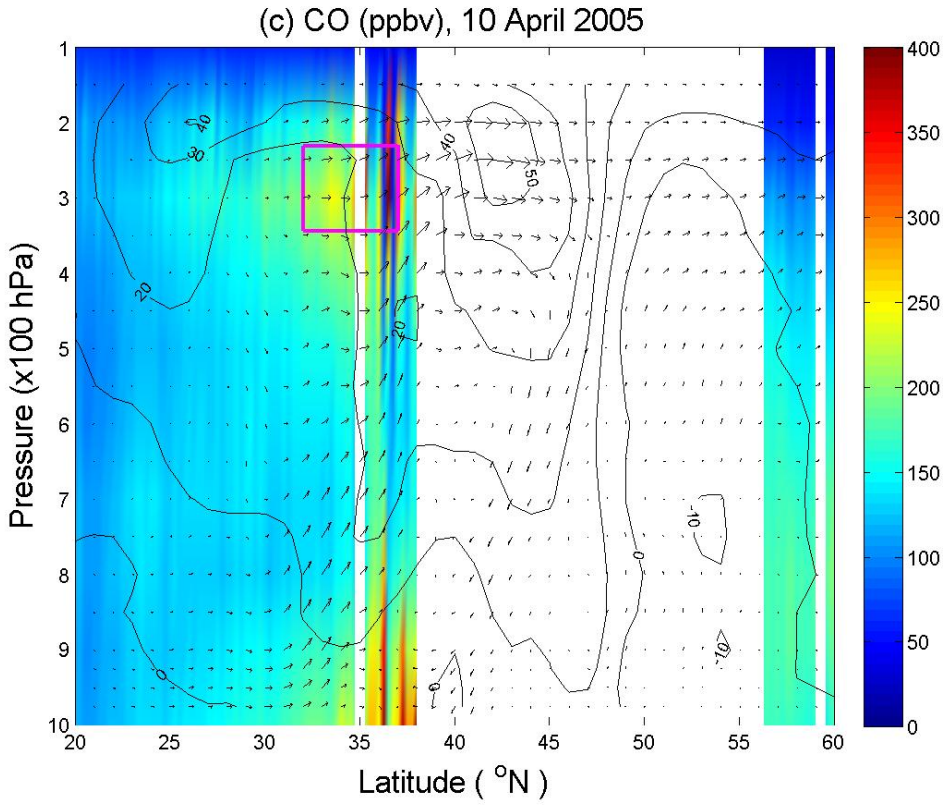

Fig. 6. A latitude-altitude cross section of MOPITT CO averaged between the two blue dashed lines in Fig.4 on (a) June 6, 2003, (b) March 18, 2004, and (c) April 10, 2005. The contour lines indicate U wind speed (m s^{-1}). Vectors are for wind directions in V and W. For a better illustration, W is enlarged by a factor of 100. The pink box(es) in (a) and (c) indicate the locations where particles were released and backward trajectories were simulated using FLEXPART (see text for detail).

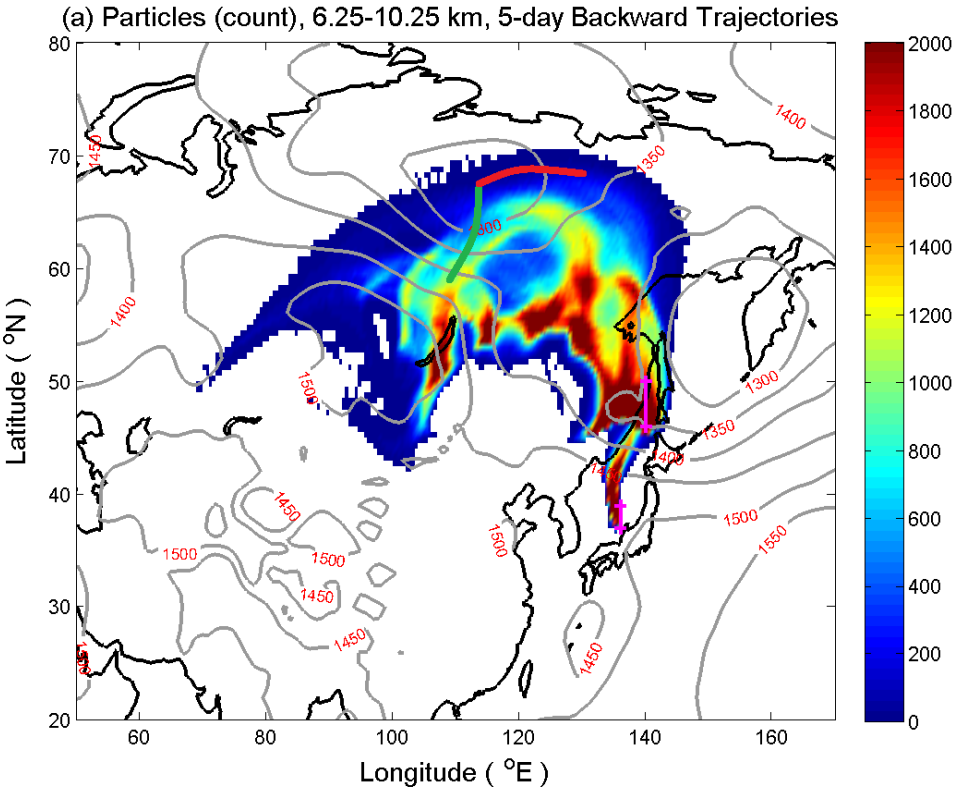
(a) Particles (count), 6.25-10.25 km, 5-day Backward Trajectories
Latitude (°N)
Longitude (°E)
80
70
60
50
40
30
20
60
80
100
120
140
160
2000
1800
1600
1400
1200
1000
800
600
400
200
0
1400
1350
1300
1450
1500
1550

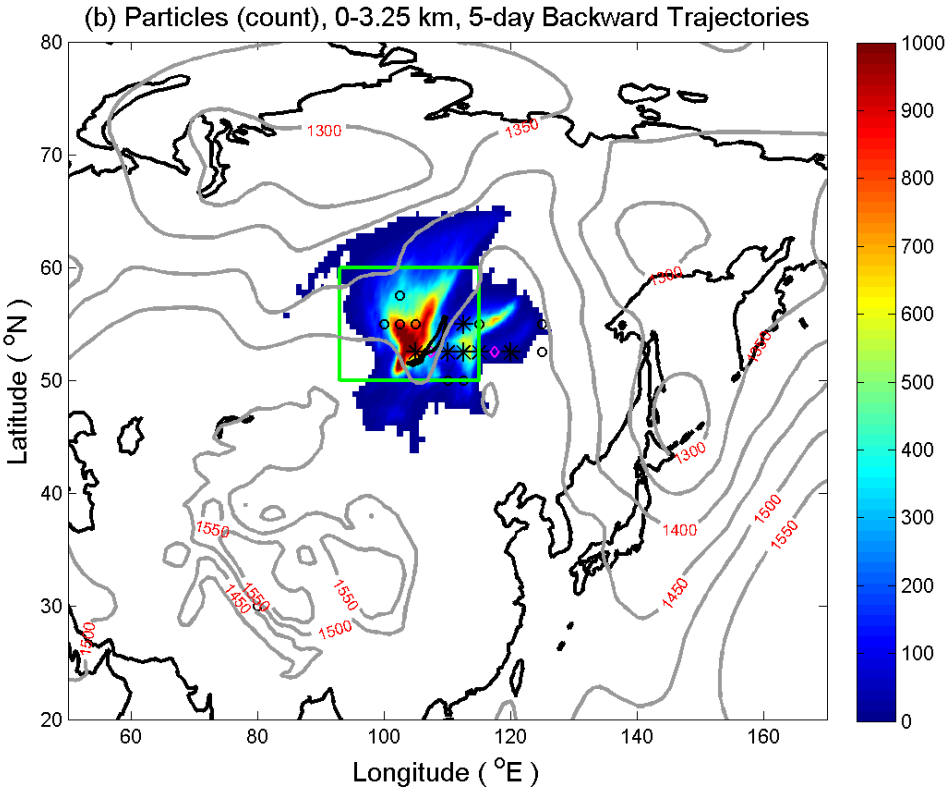
(b) Particles (count), 0-3.25 km, 5-day Backward Trajectories
Latitude (°N)
Longitude (°E)
80
70
60
50
40
30
20
60
80
100
120
140
160
1000
900
800
700
600
500
400
300
200
100
0
1300
1350
1400
1450
1500
1550

Fig. 7. (a) Particle distribution between 6.25-10.25 km (~550-250 hPa) during June 1-6, 2003. The particles were released from two locations (in pink lines) around 400 hPa (also see Figs. 4a and 6a) on June 6, 2003 and backward trajectories were calculated. The contour lines are the geopotential heights at 850 hPa on June 3, 2003. A cold front and a warm front are indicated by green and red lines, respectively. (b) The same as (a), but between 0-3.5 km. The contour lines are the geopotential heights at 850 hPa on 2 June 2003. The circles, diamonds, and stars denote daily mean fire counts of 20-100, 100-300, and 300-500 per 2.5×2.5 °grid area, respectively, from May 31 to June 6.

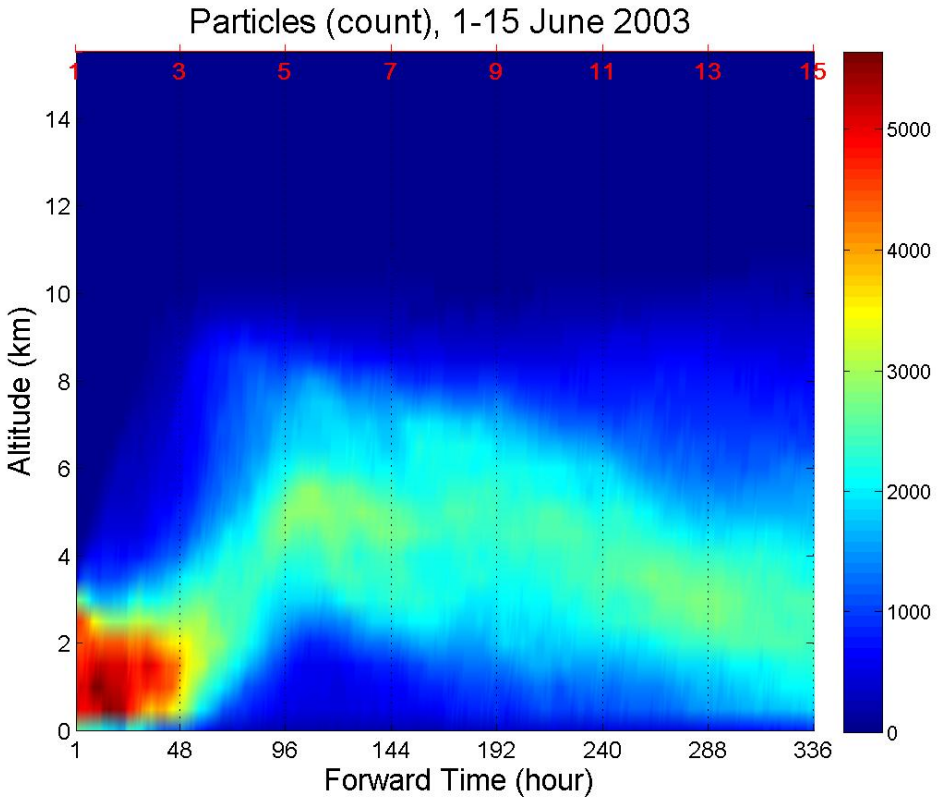

Fig. 8. Vertical distribution of particles, varying with time from 1 June 2003 at 0 UTC to 16 June 2003 at 0 UTC. The particles were released from fire regions in Fig. 7b from the surface to 3 km on 1 June 2003 and forward trajectories were calculated (15 days). The forward time (in hour) and date (in June) are indicated in the x-axis on the bottom and the top, respectively.

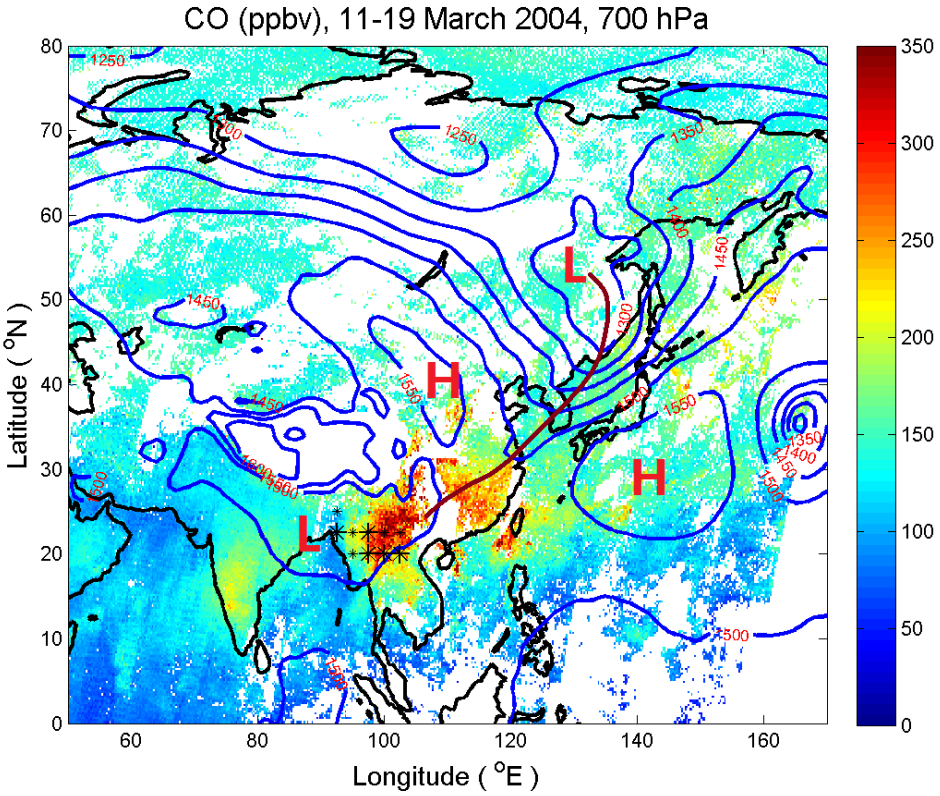

Fig. 9. MOPITT CO mixing ratio at 700 hPa from 11-19 March 2004, overlaid with the geopotential height at 850 hPa on 17 March 2004 in blue contour and with a front shown by brown solid line. The large and small stars denote daily mean fire counts of 100-200 and over 200 per 2.5×2.5 °grid area during the period, respectively. “L” and “H” indicate a low and high pressure system, respectively.

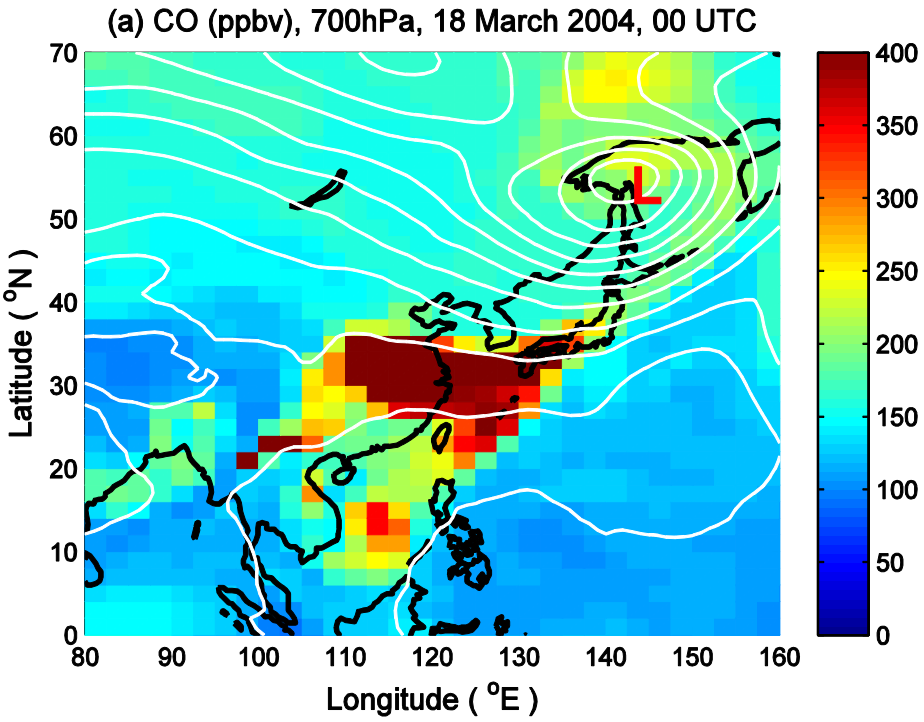
(a) CO (ppbv), 700hPa, 18 March 2004, 00 UTC
Latitude (°N)
Longitude (°E)
70
60
50
40
30
20
10
0
80
90
100
110
120
130
140
150
160
400
350
300
250
200
150
100
50
0
L

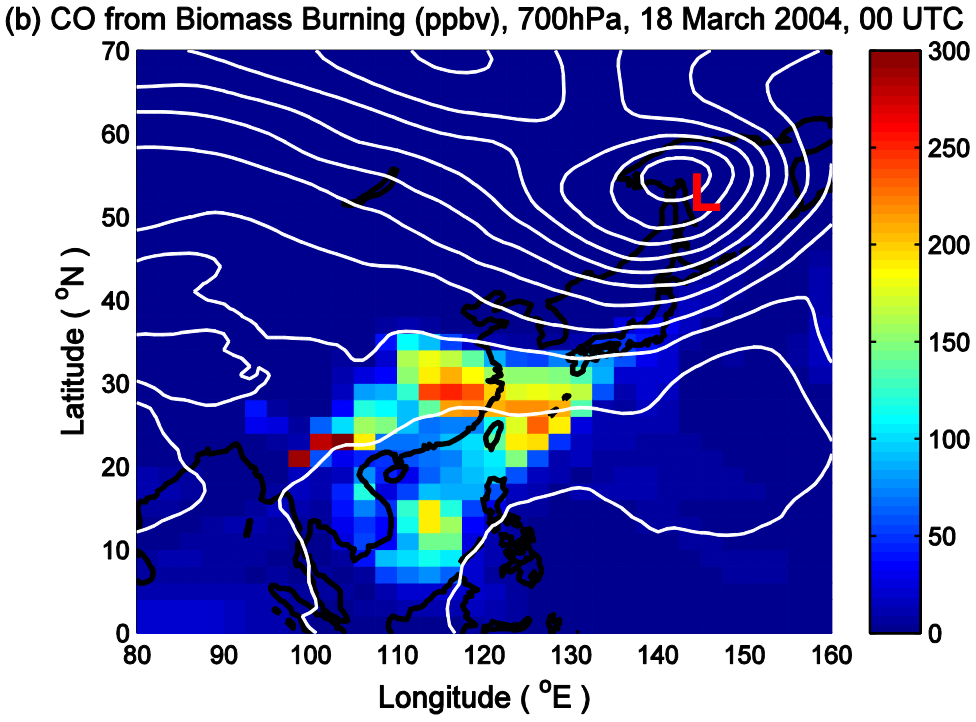
(b) CO from Biomass Burning (ppbv), 700hPa, 18 March 2004, 00 UTC
Latitude (°N)
Longitude (°E)
70
60
50
40
30
20
10
0
80
90
100
110
120
130
140
150
160
300
250
200
150
100
50
0
L

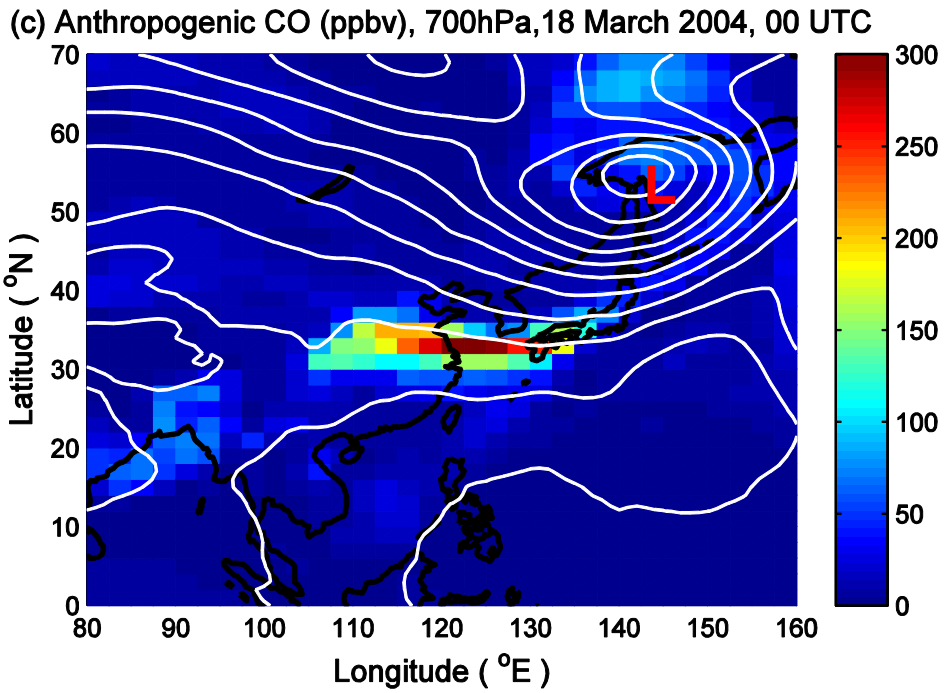

Fig. 10. (a) CO, (b) CO from biomass burning, and (c) CO from the anthropogenic source on March 18, 2004 at 0 UTC, simulated by GEOS-Chem. The geopotential height at 700 hPa is indicated with white lines. “L” indicates a low pressure system.

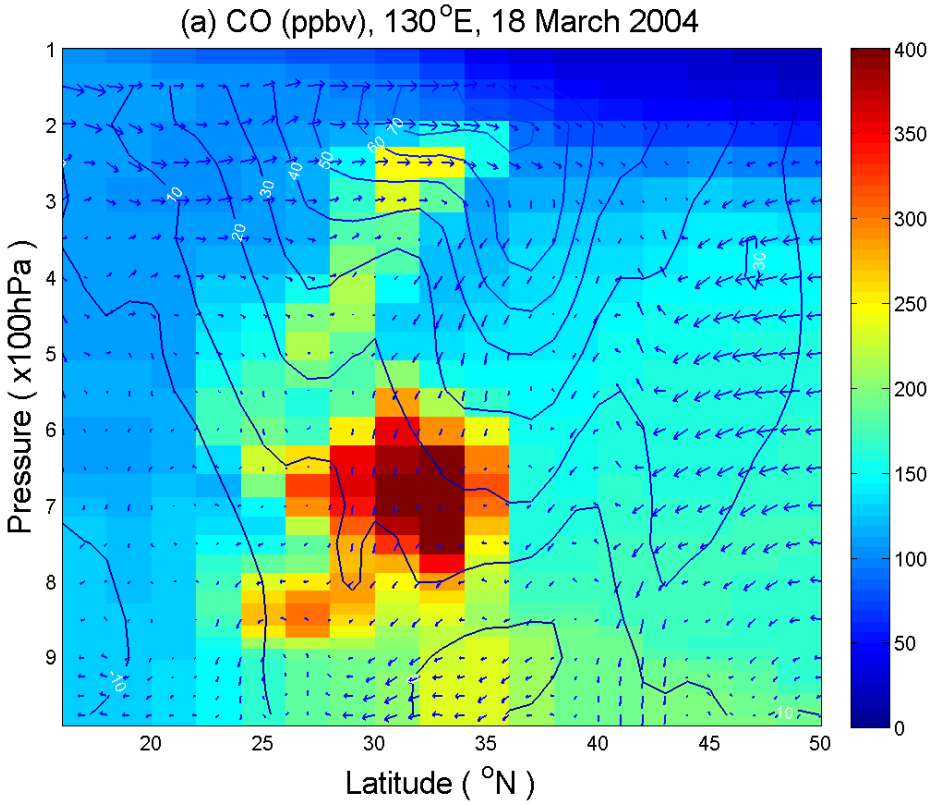
(a) CO (ppbv), 130°E, 18 March 2004
Pressure (x100hPa)
Latitude (°N)
1
2
3
4
5
6
7
8
9
20
25
30
35
40
45
50
400
350
300
250
200
150
100
50
0

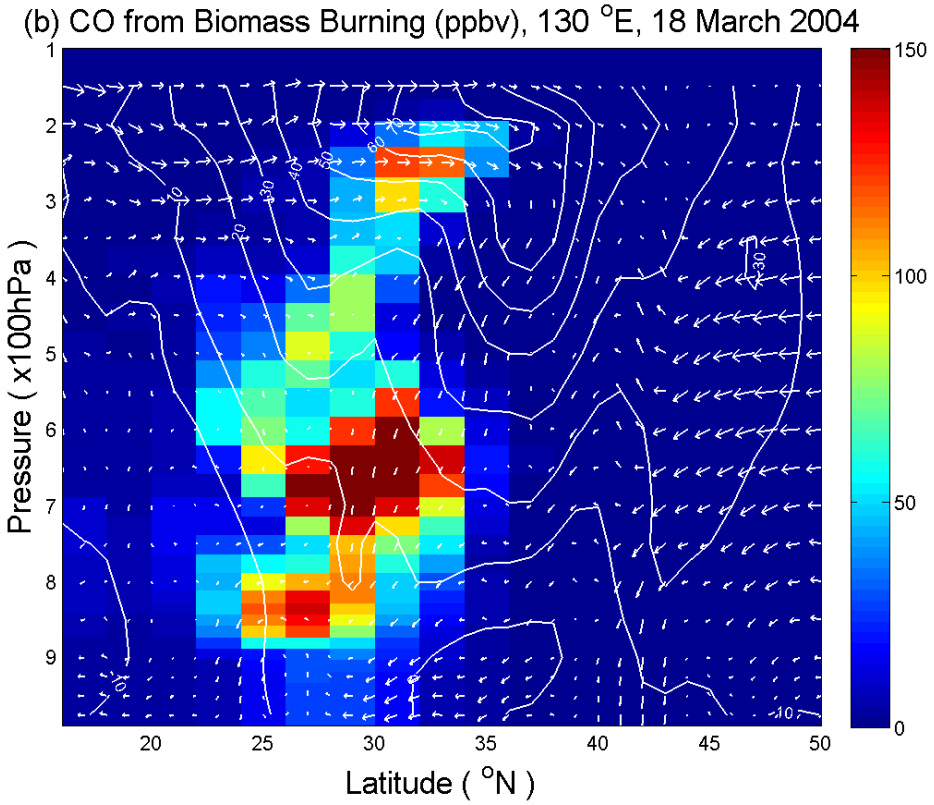
(b) CO from Biomass Burning (ppbv), 130 °E, 18 March 2004
Pressure (x100hPa)
Latitude (°N)
1
2
3
4
5
6
7
8
9
20
25
30
35
40
45
50
150
100
50
0

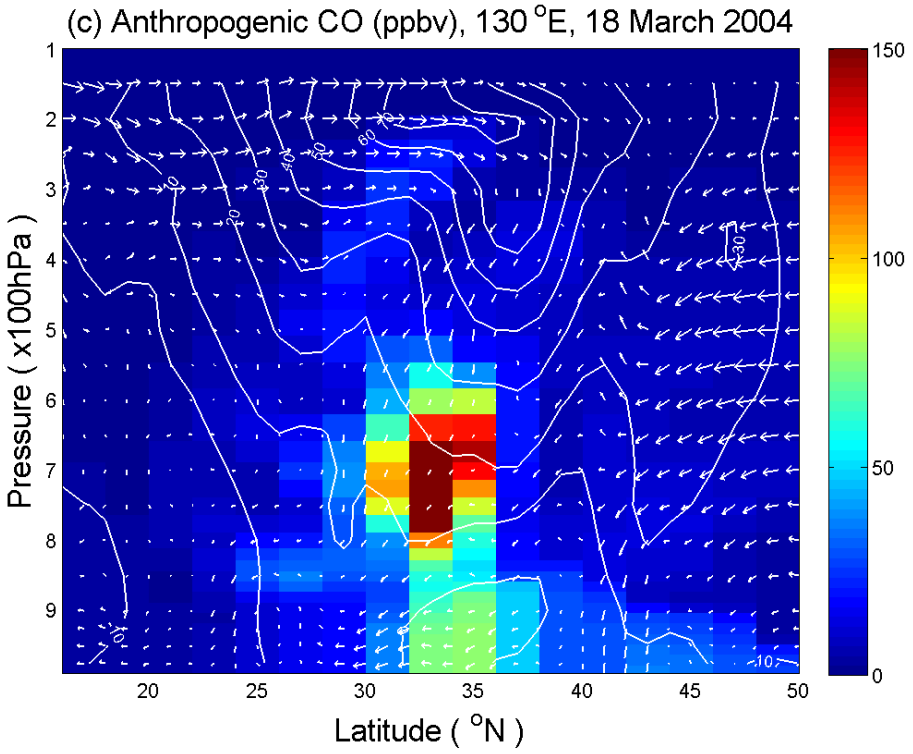

Fig. 11. Latitude-altitude cross sections along 130°E of (a) CO, (b) CO from biomass burning, and (c) anthropogenic CO on March 17, 2004 at 6 UTC, simulated by GEOS-Chem. The contour lines indicate U wind speed (m s^{-1}). Vectors are for wind directions in V and W. For a better illustration, W is enlarged by a factor of 100.

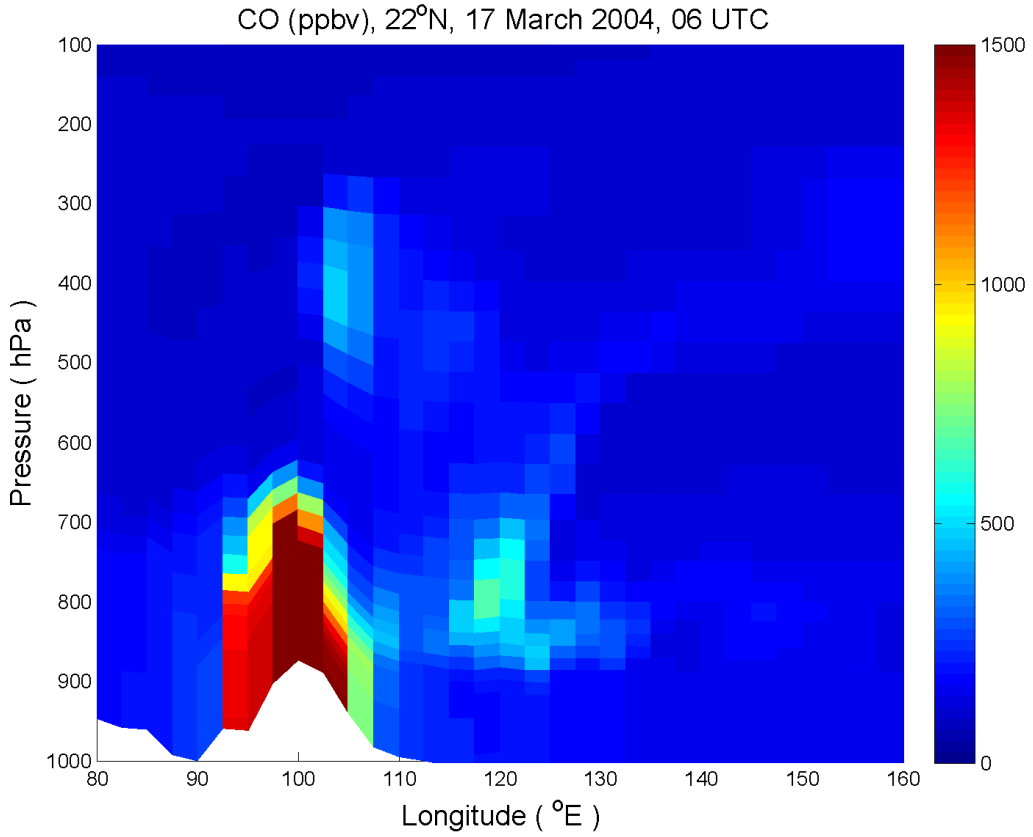

Fig. 12. A longitude-altitude cross section of CO along 22°N on March 17, 2004 at 6 UTC, simulated by GEOS-Chem. The topography of the Hengduan Mountains is indicated in white.

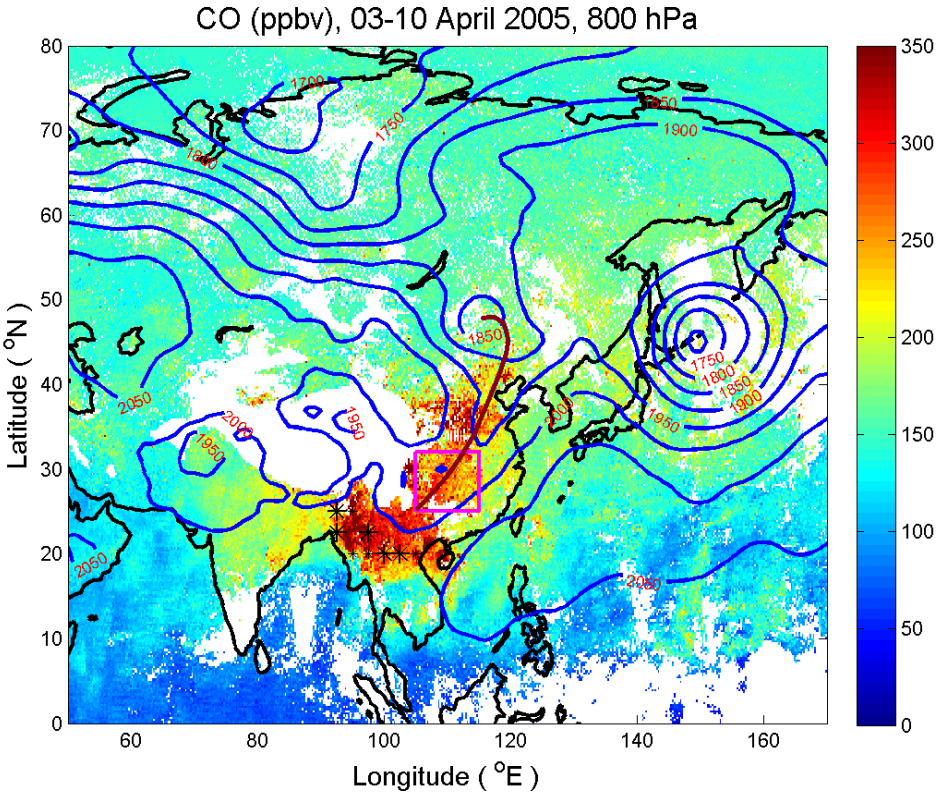

Fig. 13. MOPITT CO mixing ratio at 800 hPa from April 3-10, 2005, overlaid with the geopotential height at 850 hPa on April 9, 2005 at 0 UTC in blue contour and with a front in brown solid line. The large and small stars denote daily mean fire counts of 100-200 and over 200 per 2.5×2.5 °grid area during the period, respectively. The boxed area was identified as a major CO source region from the FLEXPART simulation (see text for detail).

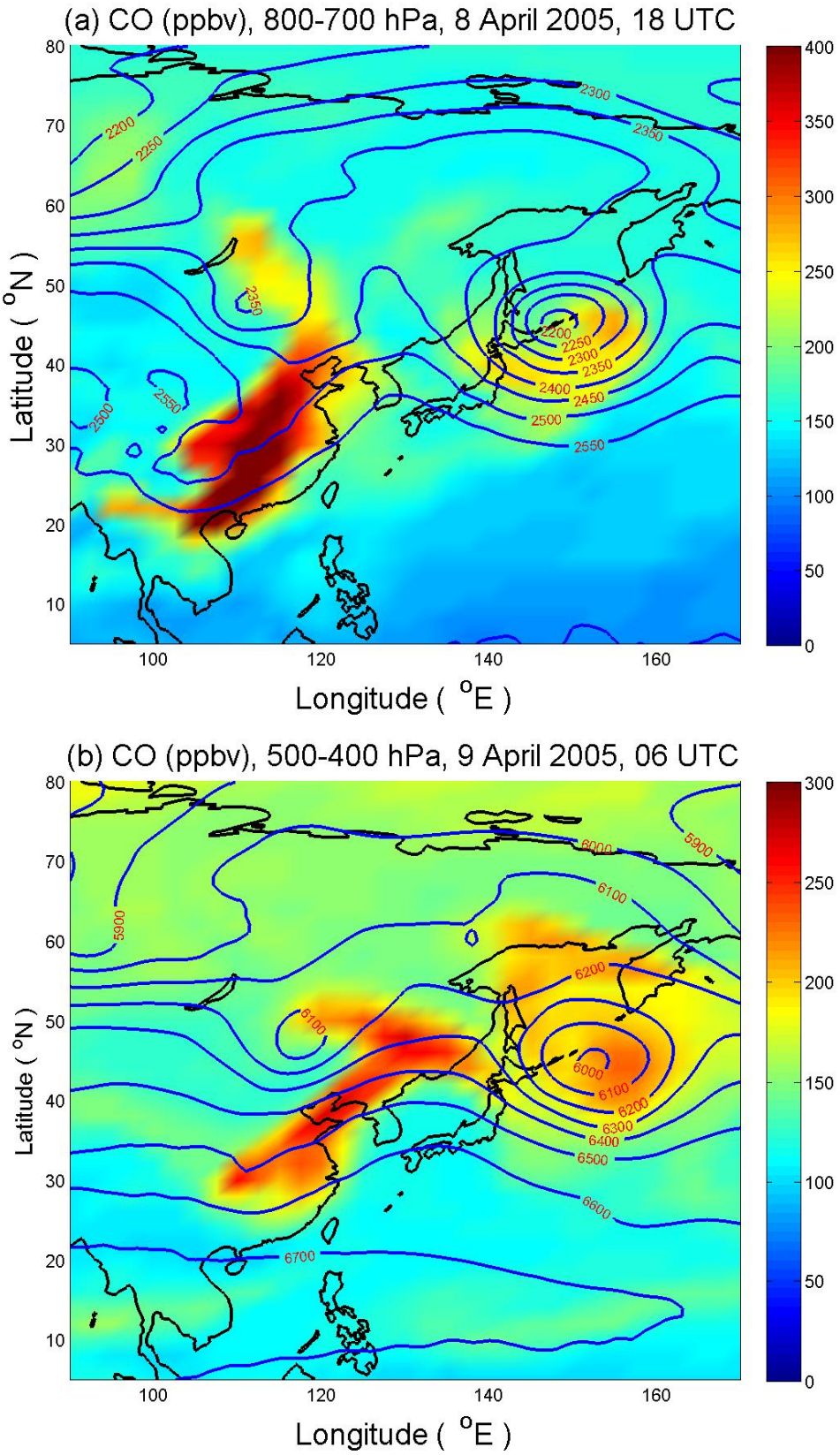
(a) CO (ppbv), 800-700 hPa, 8 April 2005, 18 UTC
Latitude (°N)
Longitude (°E)
(b) CO (ppbv), 500-400 hPa, 9 April 2005, 06 UTC
Latitude (°N)
Longitude (°E)

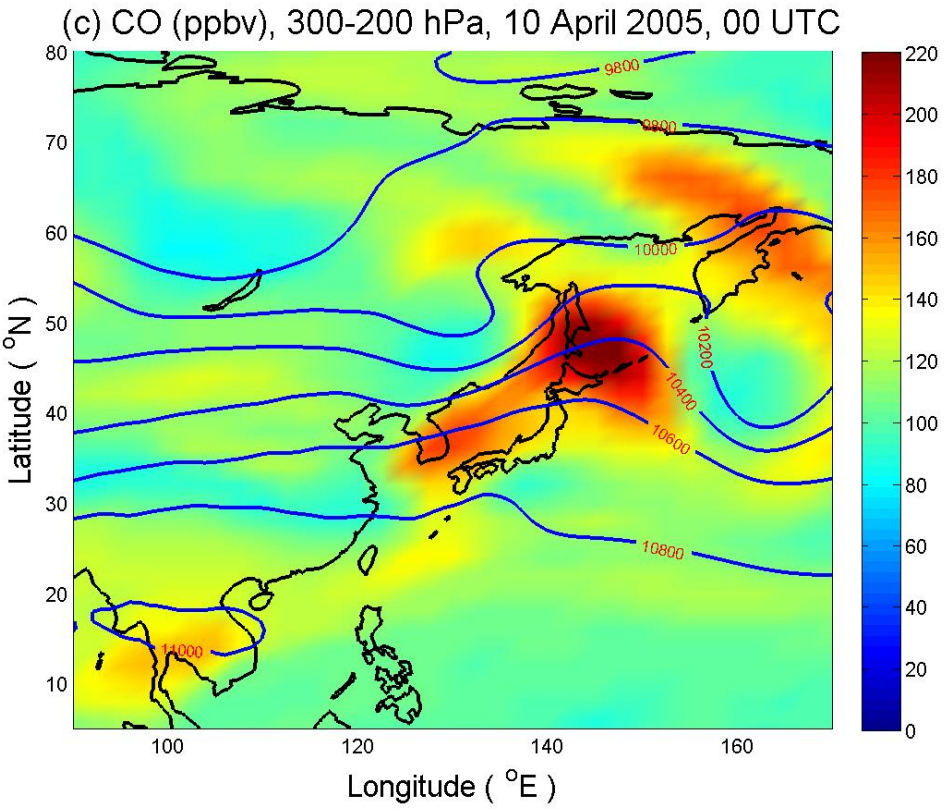

Fig. 14. The GEOS-Chem simulated CO (a) on April 8, 2005 in the lower troposphere (800-700 hPa), (b) on April 9 in the middle troposphere (500-400 hPa), and (c) on April 10 in the upper troposphere (300-200 hPa). The contours are the geopotential height at 850, 450, and 250 hPa, respectively.

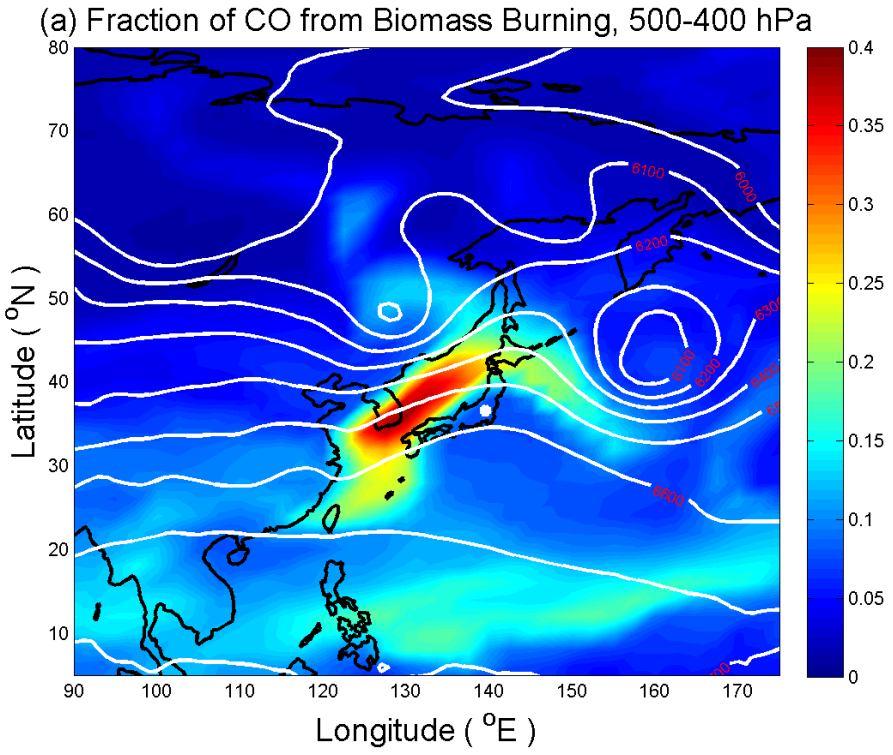
(a) Fraction of CO from Biomass Burning, 500-400 hPa
Latitude (°N)
Longitude (°E)
80
70
60
50
40
30
20
10
90
100
110
120
130
140
150
160
170
0.4
0.35
0.3
0.25
0.2
0.15
0.1
0.05
0
6100
6000
6200
6600

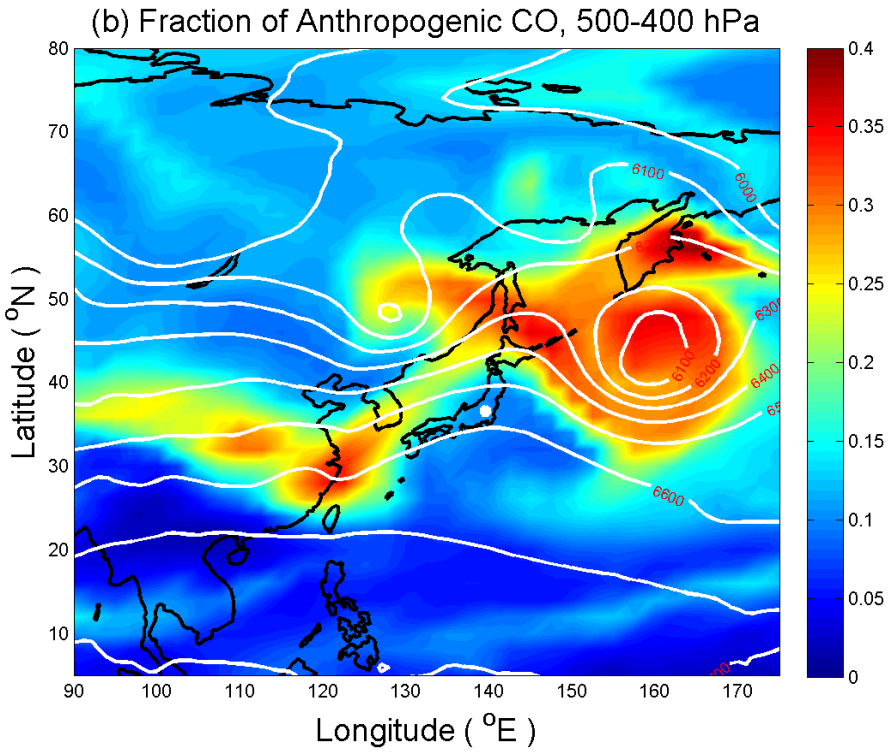
(b) Fraction of Anthropogenic CO, 500-400 hPa
Latitude (°N)
Longitude (°E)
80
70
60
50
40
30
20
10
90
100
110
120
130
140
150
160
170
0.4
0.35
0.3
0.25
0.2
0.15
0.1
0.05
0
6100
6000
6200
6600

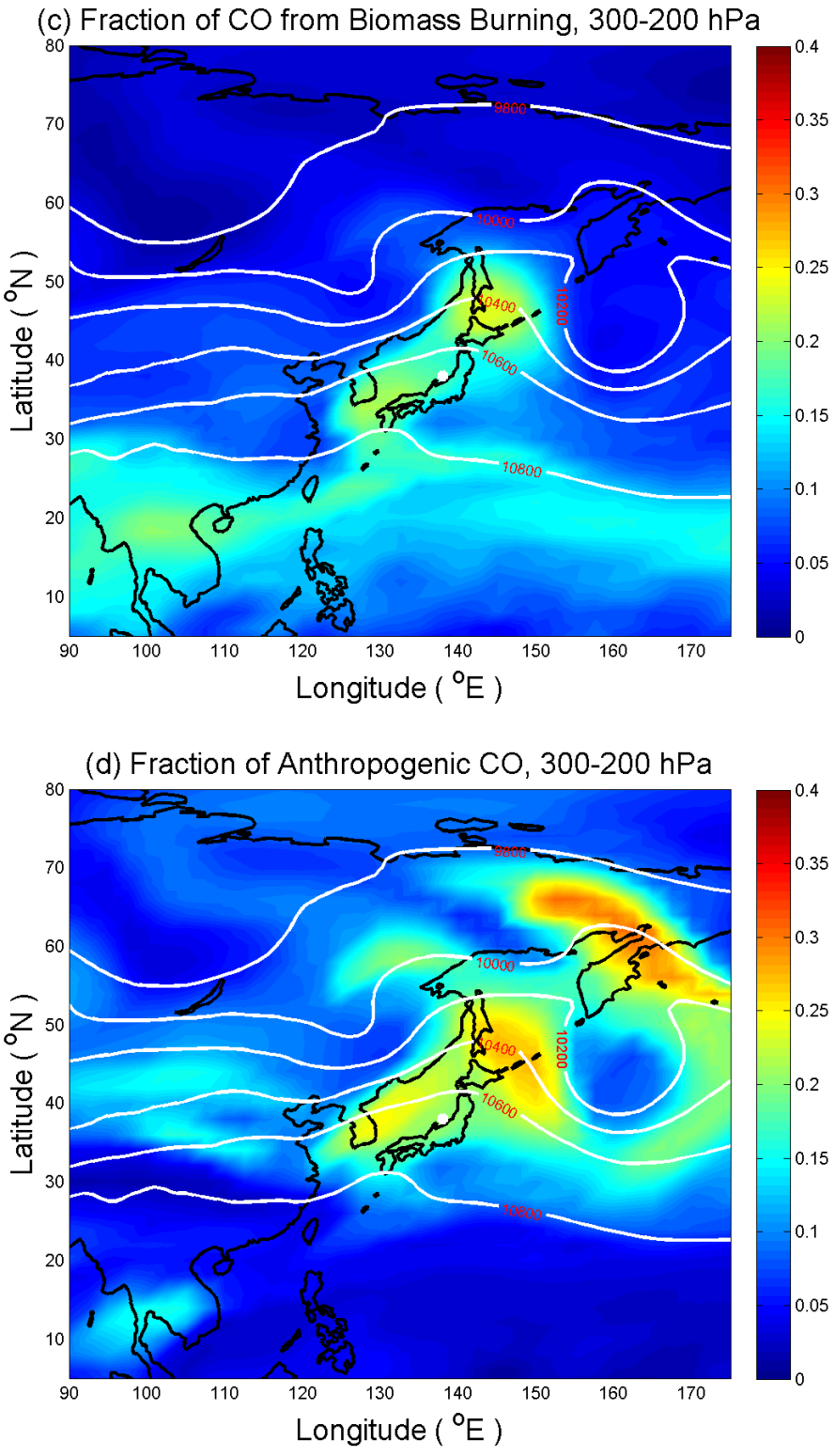

Fig. 15. The GEOS-Chem simulated fractional CO (a) from biomass burning and (b) from the anthropogenic source on April 10, 2005 at 00 UTC in the middle troposphere (500-400 hPa). (c) and (d) are the same as for (a) and (b), respectively, but in the upper troposphere (300-200 hPa). The geopotential height at 450 and 250 hPa is overlaid with the CO images in the middle and upper troposphere, respectively. White dots indicate the location of MOZAIC measurements.